High-precision sulfur isotope composition of enstatite meteorites and implications of the formation and evolution of their parent bodies

C. Defouilloy[a,b, 1,2], P. Cartigny[a], N. Assayag[a], F. Moynier[c, d], J.-A. Barrat[e]

[a]Géochimie des Isotopes Stables, Institut de Physique du Globe de Paris, Sorbonne Paris Cité, Univ. Paris Diderot, UMR 7154 CNRS, 1 rue Jussieu, 75238 Paris, France

[b]Laboratoire de Minéralogie et Cosmochimie du Muséum, Muséum National d'Histoire Naturelle, Paris, UMR 7202, 61 rue Buffon, 75005, Paris, France

[c]Cosmochimie, Astrophysique et Géophysique Expérimentale, Institut de Physique du Globe de Paris, Sorbonne Paris Cité, Univ. Paris Diderot, UMR 7154 CNRS, 1 rue Jussieu, 75238 Paris, France

[d]Institut Universitaire de France, Paris, France

[e]U.B.O.-I.U.E.M., CNRS UMR 66538 (Domaines Océaniques), Place Nicolas Copernic, 29280 Plouzané Cedex, France

[1]Current address: WiscSIMS, Department of Geoscience, University of Wisconsin-Madison, Madison, WI 53706, USA

[2]Corresponding author. defouilloy@ipgp.fr

Abstract

In order to better understand the formation and evolution of their parent bodies, the three isotope ratios of sulfur were analyzed in 33 enstatite meteorites (24 enstatite chondrites and

© 2015. This manuscript version is made available under the Elsevier user license
http://www.elsevier.com/open-access/userlicense/1.0/

9 aubrites). The results show that on average all enstatite chondrite groups are enriched in the lightest isotopes compared to other chondrite groups, with means of $\delta^{34}S$ of -0.28 ± 0.22 ‰ for EH3/4, -0.16 ± 0.16 ‰ for EH5, -0.32 ± 0.15 ‰ for EL3, -0.67 ± 0.16 ‰ for EL6 and -0.64 ± 0.00 ‰ for EL7 (all 1σ). Aubrites show a larger isotope variability in their composition, with a $\delta^{34}S$ varying from -1.350‰ to +0.154 ‰. Contrary to previously published results, our data show a distinct composition for EL6 compared to other enstatite chondrites. This could be related to an impact-induced loss of isotopically heavy oldhamite ($\delta^{34}S$ = by 3.62 ± 3.02 ‰ (1σ)) on the EL parent body. Although the bulk sulfur in both enstatite meteorites and aubrites does not show any significant $\Delta^{33}S$ and $\Delta^{36}S$, the oldhamite fraction shows clear evidence of mass independent fractionation on the $^{36}S/^{32}S$ ratio (in 3 out of 9 analyzes, $\Delta^{36}S$ up to +2.2‰), a signal that is not correlated to any $^{33}S/^{32}S$ anomaly (in 1 out of 9 analyzes, $\Delta^{33}S$ down to -0.085‰). Though a nebular or photochemical origin cannot be ruled out, the most plausible mechanism to produce such isolated non-mass dependent $^{36}S/^{32}S$ anomalies would be a contribution of $FeCl_2$ containing excesses of ^{36}S due to the decay of ^{36}Cl to the leached oldhamite fraction. Even though the sulfur isotopic composition measured in enstatite meteorites is distinct from the Bulk Silicate Earth (BSE), the isotopically lightest samples of EL6, EL7 and aubrites are approaching the isotopic composition of the BSE and enstatite meteorites remain the meteorites with the sulfur isotopic composition the closest to the terrestrial one.

1. INTRODUCTION

Enstatite meteorites comprise two groups of meteorites: enstatite chondrites, which are undifferenciated (primitive) meteorites, and aubrites, which are also referred to as enstatite achondrites, and are differentiated material.

As shown by their mineral assemblages and compositions enstatite meteorites are the most reduced meteorites (Mason 1965, Keil 1968, Rubin 1984, Brett & Keil 1986, Weisberg & Kimura 2012, Barrat et al. 2014). This is attested by their major silicate phase which is near-pure enstatite (≈ 50 wt% of total sample), with FeO < 1%. Their amount of FeNi metal (≈ 25 wt%) is higher than in other chondrite groups and the metal phase contains up to 2 wt% Si. Other important phases include troilite and plagioclase. The exceptionally reduced environment of their formation leads most lithophile elements to behave as chalcophile (El Goresy, 1988), and therefore to the formation of a large variety (0.1 to 1 %) of unusual sulphides, including oldhamite (CaS), niningerite ([Mg, Fe, Mn]S), alabandite (MnS) and rare minerals such as osbornite (TiN), sinoite (Si_2N_2O), daubreelite ($FeCr_2S_4$), caswellsilverite ($NaCrS_2$) and perryite ($[Ni,Fe]_8[Si,P]_3$) are further illustration of their very reduced character.

The enstatite chondrites are commonly subdivided into 2 sub-groups according to their amount of metallic Fe: EH (Fe-rich enstatite chondrites) and EL (Fe-poor enstatite chondrites) (Keil 1968, Sears 1980, Kallemeyn & Wasson 1983). It is also worth noting that EH are characterised by the occurrence of alabandite, while EL contain niningerite instead as well as various alkali sulfides (Lin & El Goresy 2002, Weisberg & Kimura 2012). In addition, Lin & El Goresy (2002) have given several petrographic evidence that the EH parent body had to form in even more reduced conditions than the EL parent body, with a lower oxygen and

a higher H_2S fugacity, resulting in a higher Si content in kamacite and perryite, and alkali enrichment in sulphides in unequilibrated EL3 compared to their EH3 counterparts. Like other chondrites, enstatite chondrites present various degrees of metamorphism, from the more primitive group, noted 3, to the most metamorphosed, noted 6 (or 7). Yet, due to their very specific mineralogies, it can be challenging to assess precisely the exact degree of metamorphism and uncertainty remains regarding the classification of enstatite chondrites (Quirico et al. 2011). It is to be noted that there are no hydrous metamorphosed enstatite. This is primarily the consequence that no hydrous phase exists, H being dissolved in the metal phase.

Interestingly, enstatite chondrites are the only undifferentiated meteorites to possess a well-identified differentiated counterpart, the aubrites. Aubrites are for the most part fragmental breccias or regolith impact breccias, with the exception of 6 samples representing impact melts (Casanova et al. 1993, Lorenzetti et al. 2002, Miura et al. 2007). Besides enstatite, their main minerals are albitic plagioclase, diopisde and forsterite. Based on similar O isotopic compositions and major element content, they are thought to originate from an enstatite chondrite-like parent body, but neither from the EH nor the EL parent bodies (Keil 2010). No study has reported a comparison of O fugacity in aubrites with EL and EH. However, their mineralogical composition and possibly complementary Zn isotopic composition tends to show that aubrites are closer to EL than EH (Watters & Prinz 1979, Rubin 1984, Moynier et al. 2011).

The origin of enstatite meteorites and their parent bodies and the genetic relationships between all the sub-groups remain partially unsolved today. There are several arguments in

97 favour of a common origin of enstatite chondrites. For example, they have several
98 remarkable features that distinguish them from any other meteorite groups. They have a
99 distinct mineralogy, with a wide variety of sulfides and metals, reflecting their highly reduced
100 environments of formation. They also have similar oxygen isotopic compositions (Clayton &
101 Mayeda 1996, Herwartz et al. 2014). It is therefore likely that they share a common origin.
102 Several authors have favoured a common parent body for all the enstatite chondrites, EL
103 and EH (Clayton and Mayeda, 1996, Kong et al. 1997). This is corroborated by the fact that
104 they are all completely dry (there are no enstatite chondrites of petrologic types 1 or 2) and
105 the high melting temperature of enstatite. Yet some incompatibilities have been emphasized
106 (Keil 1968, Brett & Keil 1986, Lin & El Goresy 2002, Keil 2010). In particular, Lin and El Goresy
107 (2002) showed that the chemical and petrography of the EH and EL were incompatible with
108 a common parent body. EH have a higher Mg/Si ratio than the EL (Keil et al. 1968). EL and EH
109 also have very distinct cooling rates and heating histories, suggesting distinct parent bodies
110 (Zhang et al. 1995, Lin & El Goresy 2002).
111
112 The chemical, and isotopic similarities between enstatite meteorites that were previously
113 used as evidence for common parent body are now re-interpreted in terms a common
114 environment of formation for the different parent bodies (as attested by the mineralogy of
115 the meteorites. Rubin et al. 2009). Even though it is now generally assumed that enstatite
116 meteorites originate from at least four different parents bodies – one for the EL, one for the
117 EH, and 2 for the aubrites (one for the Shallowater meteorite, and another parent body for
118 all the other aubrites) – a few studies have pointed out the peculiarity of EL6 compared to
119 EL3 and EH in their REE content (Rubin et al. 2009, Barrat et al. 2014) and zinc isotopic

120 composition (Moynier et al. 2011), leading to the question whether they could originate
121 from an additional distinct parent body.
122
123 Both enstatite meteorites and the Earth (as well as other terrestrial planets) formed in a
124 reduced environment, which suggests a possible link between them (Javoy et al. 2010,
125 Sanloup et al. 1999). Isotopic similarities between the Earth and enstatite meteorites are
126 remarkable, the most striking observation being the oxygen isotopic composition (Clayton et
127 al. 1984, Clayton & Mayeda 1996, Newton et al. 2000, Herwartz et al. 2014). Isotopic
128 similarity between the Earth and enstatite meteorites now extend to many additional
129 elements such as Zn (Moynier et al. 2011), N (Javoy & Pineau 1983, Cartigny et al. 1997), Mo
130 (Dauphas et al. 2004), Ru (Dauphas et al. 2004), Cr (Birck et al. 1999, Trinquier et al. 2007a),
131 Sr (Moynier et al. 2010, 2012), Ti (Trinquier et al. 2007b) and Ca (Valdes et al. 2014). These
132 similarities has led to the idea that, contrary to first assumptions, the Earth was not built
133 from a majority of ordinary chondrites and carbonaceous chondrites -like material, but
134 primarily from enstatite-like material (Javoy 1998, Javoy et al. 2010). However, the Mg/Si
135 ratio of bulk enstatite chondrites is much lower than that of BSE, and the Si isotopic ratio
136 measured in all enstatite meteorites is significantly different from Earth (Fitoussi & Bourdon
137 2012, Savage & Moynier 2013), though Dauphas et al. (2015) have recently shown that
138 Mg/Si ratio was dictated by the the condensation sequence of forsterite in the solar nebula.
139 Earth and enstatite meteorites might also slightly differ in their Ti isotopic composition
140 (Trinquier et al. 2009, Zhang et al. 2012) as well as Ca isotopic composition (Simon &
141 DePaolo 2010), though the latter was recently proved disputable by Valdes et al. (2014).
142 Finally, a recent study by Herwartz et al. (2014) revealed small but significant differences in
143 the ^{17}O isotopic compositions of Earth and enstatite meteorites: 59 ± 8 ppm (0.059 ±

144 0.008 ‰) for EL and 35 ± 10 ppm (0.035 ± 0.01 ‰) for EH. Though it seems undeniable that
145 enstatite meteorites share a lot of features with the Earth, building the Earth solely from
146 enstatite-like material is not free of difficulties.
147
148 Sulfur is present in enstatite meteorites in significant quantity (≈ 4-5 wt% S) (Keil et al. 1968).
149 Having 4 isotopes (^{32}S, ^{33}S, ^{34}S, ^{36}S), it allows the distinction of equilibrium and kinetic effects
150 and the identification of mass independent isotopic fractionation (MIF). A scarce number of
151 sulfur isotopic compositions have been measured in enstatite chondrites (Gao & Thiemens
152 1993a) and aubrites (Rai et al. 2005), including significant MIF reported in the aubrite Norton
153 County (Rai et al. 2005). To better discuss the differences and relationships between the
154 different groups of enstatite meteorites and to better apprehend the link between the
155 enstatite meteorites and the building material of the Earth, we report the S isotopic
156 composition of 33 enstatite chondrites and aubrites, to create a precise spectrum of the S
157 isotopic variations and possible MIF in all the enstatite-bearing bodies.
158
159
160 **2. SAMPLES AND METHODS**
161
162 33 samples of enstatite meteorites, from all groups and metamorphism degrees have been
163 analysed: 2 EL3 (Mac 88 136, Mac 02 837), 9 EL6 (Hvittis, Khaipur, Eagle, North West Forest,
164 Lon 94 100, Happy Canyon, EET 92 063, NWA 974, Pillistfer, Atlanta, Blithfield), 2 EL7 (Happy
165 Canyon, Ilafegh 009), 8 EH3 (Indarch, Qinz-Zhan, Gro 95 517, Abee, Kota-Kota, Alha 77 295,
166 Mil 07 028, Itqiy, Sahara 97 096), 3 EH5 (St Sauveur, LA 02 225, St Mark's) and 9 Aubrites
167 (Norton County, Khor Temiki, Shallowater, Bishopville, Cumberland Falls, Aubres, Bustee,

Mayo Belwa, Pena Blanca). Two samples, North West Forest (EL6) and Itqiy (EL7-an), did not release any sulfur.

2.1. Analytical techniques

2.1.1. Extraction of reduced sulfur

Samples were obtained either as fine powders or as cm-size chunks of rocks that were subsequently crushed into powder. For bulk reduced sulfur extraction about 20 mg of powder was used in each experiment. When enough material was available, a replica or two were processed. The powered samples were poured in a glass reaction vessel with 20 ml of chrome reduction solution (≈ 30 % $Cr(III)Cl_3$ + 15 % Zn + 55 % HCl 0.6 N, see Canfield et al. 1986). 5 ml of HCl 6N were added to the mixture to ensure an acidic condition, which enhances the reaction rate. The flasks were heated to boiling temperature for 3 hours under a flux of N_2. Hydrogen sulfide was swept out with a stream of nitrogen gas, washed in distilled water, and collected in a silver nitrate solution. Ag_2S was rinsed with distilled water and then dried for 24 hours.

As detailed previously (e.g. Canfield et al. 1986) extensive tests on pure FeS_2 original material has shown that our settings for the chemical extraction of sulfides ensure a close to 100% yield and do not create any significant fractionation of sulfur isotopes.

Weighed aliquots of Ag_2S samples wrapped in Al foils, are introduced in nickel bombs, evacuated and fluorinated with purified F_2 at 250° overnight. The reaction releases SF_6 which is then purified by cryogenic separation and gas chromatography (1/8 in. diameter column of a 6 ft 5A molecular sieve followed by a 8 ft Haysep Q column. Ono at al 2006). Purified SF_6 is then quantified using a capacitance manometer (to check for fluorination yield) and analyzed by mass spectrometry.

Several large samples were obtained, allowing the isotopic composition of oldhamite (CaS) to be investigated. CaS is a fragile sulphide, easily reacting with water to produce H_2S. The extraction procedure was similar to the protocol used for extracting all sulphides: 3 g of powdered sample were poured in a flask, heated at ≈ 100°C for 10 hours with 20 ml of pure water. No other reagent was added. Particular care was taken to ensure that all glassware was perfectly dry before experiment. Similarly to bulk S extraction, H_2S was produced and converted to Ag_2S.

2.2. Isotope analysis

The sulfur isotopic compositions were measured using a dual inlet Thermo Finnigan MAT 253 Mass Spectrometer at the Institut de Physique du Globe de Paris, France. M/z ratios 127, 128, 129 and 131 ratios were monitored simultaneously (respectively for $^{32}SF_5^+$, $^{33}SF_5^+$, $^{34}SF_5^+$, $^{36}SF_5^+$). The $\delta^{34}S$ values are calculated after calibration of our in-house SF_6 tank, using the international standard IAEA-S1 recommended value of Robinson (1993). As this reference material is anchored to V-CDT, the $\delta^{34}S$ values measured in this study are all given respect to

V-CDT. There is no international calibration for neither $\Delta^{33}S$ nor $\Delta^{36}S$ and there are given with respect to our SF_6 tank and were recalculated accordingly via the relations:

$$\Delta^{33}S = \delta^{33}S + 1000 \times [(\delta^{34}S/1000 +1)^{0.515} -1] \quad (1)$$

$$\Delta^{36}S = \delta^{36}S + 1000 \times [(\delta^{34}S/1000 +1)^{1.9} -1] \quad (2)$$

The quality of the measurements is estimated on the basis of the long term reproducibility of IAEA-S1 and IAEA-S2 reference materials (Table 1, Appendix A). Repeated analyses conducted during completion of this work gave, for IAEA-S1, $\delta^{34}S$ = -0.378 ± 0.17 ‰, $\Delta^{33}S$ = 0.117 ± 0.006 ‰ and $\Delta^{36}S$ = -0.36 ± 0.28 ‰ (all 1σ, n=17) and $\delta^{34}S$ = 22.01 ± 0.40 ‰, $\Delta^{33}S$ = 0.03 ± 0.07 ‰ and $\Delta^{36}S$ = -0.20 ± 0.3 ‰ (all 1σ, n=20). Those values are statistically indistinguishable from those given in Ono et al. (2006), Johnson et al. (2008) and Labidi et al. (2012). CDT samples were also analyzed. They gave raw values of $\delta^{34}S$ = -0.37 ± 0.2 ‰, $\Delta^{33}S$ = -0.029 ± 0.004 ‰ and $\Delta^{36}S$ = -0.129 ± 0.087 ‰ (all 1σ, n=9). To express our $\Delta^{33}S$ and $\Delta^{36}S$ results relative to V-CDT, V-CDT being assumed at zero, all results have been normalized to V-CDT using the above values and noted as $\Delta'^{33}S$ and $\Delta'^{36}S$.

Each measurement session was preceded by a zero-enrichment. In addition, two standards (IAEA-S1, IAEA-S2 or CDT) samples were analyzed at each session, one at the beginning and one at the end to assess data quality.

3. RESULTS

3.1. Bulk sulfur

Our results are presented in Table 2 and Figure 1. The S isotopic composition of EH3, EH5 and EL3 are all within uncertainties of each others. These values are in good agreement with Gao and Thiemens (1993a), except for the EL6 and EL7 groups, for which our values (respectively $\delta^{34}S$ = -0.66 ± 0.14 ‰ and $\delta^{34}S$ = -0.64 ± 0.00 ‰) are distinctively lower compared with their values ($\delta^{34}S$ = -0.24 ± 0.06 ‰, n = 3, σ = 1, Gao & Thiemens, 1993a).

Aubrites (Aubrite Main Group and Shallowater) show a mean value of $\delta^{34}S$ = -0.43 ± 0.53 ‰ $\Delta'^{33}S$ = 0.006 ± 0.037 ‰ and $\Delta'^{36}S$ = 0.041 ± 0.237 ‰. Shallowater is a particular aubrite that is thought to come from a distinct parent body (Keil 1989, 2010). As Shallowater ($\delta^{34}S$ = -0.46 ‰) does not show any distinct isotopic composition in sulfur compared with other aubrites ($\delta^{34}S$ = -0.43 ± 0.56 ‰, without Shallowater), we will not make any further distinction between the main group and Shallowater and regroup all of them in one "aubrites" entity. This merge is only made for purpose of clarity and does not imply in any way that Shallowater and the Main Group might originate from the same parent body based on S isotopic compositions.

Most of aubrites data overlap with the composition measured in enstatite chondrites, yet with several samples displaying more extreme values, between two poles, one positive ($\delta^{34}S$ = +0.154 ‰ measured in Aubres) and one negative ($\delta^{34}S$ = -1.350‰ as measured in Bishopville). Interestingly, Bishopville displays a significant difference in isotope composition between the two chunks (i.e. two distinct samples from two museums) that were analyzed from this meteorite ($\delta^{34}S$ = -1.350‰ vs. $\delta^{34}S$ = +0.215‰). This difference of 1.566 ‰ is way

beyond the overall uncertainty of our analytical protocol, and must represent a sample heterogeneity. This heterogeneity is also noticeable in the different concentrations of sulfur between those two chunks, with an S content of about 1.9 wt% and 0.1 wt% for the ^{34}S –depleted and –enriched samples respectively.

Cumberland Falls is a particular aubrite as it contains both clasts of aubritic nature and clasts from ordinary chondrite material that is thought to come from an impactor to the aubrite parent body. First analyses on undiscriminated powder from the meteorite gave a bulk composition of $\delta^{34}S$ = -0.517 ± 0.06 ‰. Subsequent analyses on specifically selected aubritic and OC clasts showed an aubrite composition much more negative, $\delta^{34}S$ = -1.903 ‰, while the OC clast showed a $\delta^{34}S$ of 0.007 ‰, in perfect agreement with an ordinary chondrite signature (Gao & Thiemens 1993a) and confirming that aubrites are also heterogeneous in S isotopes.

No obvious MIF in ^{33}S or ^{36}S is observed in the bulk fraction analyses (Figure 2), neither in enstatite chondrites nor aubrites, mean values of $\Delta'^{33}S$ and $\Delta'^{36}S$ for each group being very close to zero. There is no distinctive trend in the $\Delta'^{33}S$ or $\Delta'^{36}S$ individual analyses, though a slight dispersion of the values beyond the standard deviation can be noted.

3.2. Water soluble fraction

Twelve large samples (4 EH and 8 aubrites) were specifically analyzed to access the S isotope composition of oldhamite (Table 3, Figure 3). Nine of them released enough sulfur to allow for analysis of S isotopes, while three (all aubrites) did not release any significant amount of

sulfur. The sulfur isotopic composition of the water soluble fraction is distinctively different from the bulk S of enstatite meteorites, showing large variations between samples (with a $\delta^{34}S$ from 0.66 ‰ to 10.95 ‰) and an enrichment in all three heavy isotopes compared to bulk S compositions, with averages $\delta^{34}S$ = 3.62 ± 3.02 ‰, $\Delta'^{33}S$ = -0.024 ± 0.027 ‰ and $\Delta'^{36}S$ = 0.629 ± 0.724 ‰. Three samples (EH3 Indarch, and aubrites Norton County and Aubres) show significant ^{36}S excess (respectively $\Delta'^{36}S$ = 2.23 ‰, 1.19 ‰ and 0.91 ‰). Norton County is the only sample to show significant anomalies in both ^{36}S and ^{33}S, with a positive $\Delta'^{36}S$ (+1.185 ‰) and a negative anomaly in $\Delta'^{33}S$ (-0.085 ‰). This result contrasts with the datum of Rai et al. (2005) who measured a positive anomaly in $\Delta'^{33}S$ of 0.161 ± 0.012 ‰ in oldhamite of Norton County and $\Delta'^{36}S \approx 0$ ‰, suggesting that a given aubrite can also be isotopically heterogeneous in terms of ^{33}S isotopes, best illustrated by the water soluble fraction. To our knowledge, these isotope anomalies do not compare with other data in bulk meteorites (Antonelli et al., 2014; Hulston and Thode, 1965b).

4. DISCUSSION

4.1. Heterogeneity of the samples

Previous petrographic studies have shown that at a mm scale, samples can be very heterogeneous in their mineral composition (Mason 1965, Keil 1968, Rubin 1984, Brett & Keil 1986). This is supported by S isotopes and particularly for aubrites and EL6, which contain less sulfides than the other groups. In several cases, samples from the same chunks

311 did not contain extractable sulfides. A misstep in the chemical extraction was unlikely since
312 for samples for which enough material was available to perform replicates from the same
313 chunk, as for pyrite tests, all the results were within experimental error. It is therefore more
314 likely that these chunks did not contain any sulfide. Some of the samples that we had
315 received as powders were possibly oxidized with the clear presence of rusty material.
316 Therefore the sulfides may had been oxidized to sulfates and were not extracted by our
317 analytical method. In order to test this possibility we performed an extraction using Thode's
318 method (Thode et al. 1961) to extract sulfur from sulfates which did not yield anything either
319 (see table 2). Therefore, it is more probable that the lack of sulfur was due to the
320 heterogeneous nature of the original material (usually single chunks, or powder from a
321 single chunk), which is expected given the brecciated nature of those samples, with clasts of
322 mm to cm size. This idea is further supported by the fact that the two distinct chunks from
323 Bishopville displayed contrasted isotope compositions.
324 Although the sulfur content can be heterogeneous, the isotopic composition remains fairly
325 reproducible between different replicates of a same meteorite with a difference of less than
326 0.2 ‰ in $\delta^{34}S$, with the noticeable exceptions of Abee (EH4), which displays a variability of
327 0.377 ‰, and Bishopville (aubrite), showing a significant variation of 1.566 ‰ in $\delta^{34}S$.
328
329 **4.2. Mass independent isotopic fractionation in the water soluble fraction**
330
331 Significant MIF are observed in the water soluble fractions (Figure 4) of the analyzed samples
332 showing a clear positive $\Delta'^{36}S$ up to 2.23 ‰ for Indarch (with a corresponding $\Delta'^{33}S$ = 0.006 ±
333 0.01 ‰), and a slightly negative $\Delta'^{33}S$ of -0.085 ‰ in Norton County (with a $\Delta'^{36}S$ = 1.185 ±
334 0.1 ‰). This contrast with the bulk sulfur fraction of EL, EH and aubrites, where very

335 restricted MIF occurs with -0.009 ‰ < $\Delta'^{33}S$ < +0.021 ‰ and –0.160 ‰ < $\Delta'^{36}S$ < +0.319 ‰.
336 Oldhamite is a rare mineral only observed naturally in enstatite meteorites (chondrites and
337 achondrites). It has never been observed on terrestrial samples, nor in other meteorite
338 groups. Larimer (1968) showed that this peculiarity of enstatite meteorites is probably due
339 to a highly-reduced environment of formation, with a low oxygen fugacity (log pO_2 = 8.58 –
340 25.35/T) associated with a high C/O ratio (≈ 0.9).
341 If these anomalies were imputable to experimental errors, as bulk and water soluble
342 samples were analyzed in no particular order, they would likely appear in both S fractions
343 (bulk and water soluble) of aubrites and enstatite chondrites. However, MIF is observed only
344 among water soluble fractions. Moreover, the samples showing MIF were not analyzed
345 during the same sessions, therefore, it is rather unlikely that they could result from
346 experimental errors. This MIF signal is thus real, and specific to the water soluble fraction.
347 There are three typical explanations to generate MIF in meteorites: (1) cosmic ray spallation,
348 including the production of cosmogenic nuclides (2) photochemically-induced gas phase
349 chemical reactions and (3) stellar nucleosynthesis (Rai et al. 2005, Chakraborky et al. 2013,
350 Antonelli et al. 2014).
351
352 Spallation reactions leads to nuclides produced from interactions between highly energetic
353 particles (cosmic rays in the case of Cosmic Ray Spallation, or CRS) and a target nuclei. CRS
354 producing excess in S isotopes have only been studied in iron meteorites, where the target
355 element – Fe – is the most abundant and the irradiation ages are the longest (Hulston &
356 Thode 1965a, Hulston & Thode 1965b , Gao & Thiemens 1991). In the absence of spallation
357 studies on enstatite meteorites, iron meteorites remain the closest analogues and a
358 comparison with iron meteorites is supported by the fact that EH and EL are the richest

meteorites in iron after iron meteorites. In iron meteorites, spallation reactions is associated with a specific ratio $\Delta^{36}S/\Delta^{33}S \approx 8$, which does not match favorably our results in enstatite meteorites (Figure 4), making spallation an unlikely explanation for the observed MIF. In particular, spallation would only create positive $\Delta^{33}S$ and cannot account for our slightly negative $\Delta^{33}S$ observed in Norton County.

Ruling out cosmic ray exposure and stellar nucleosynthesis as the origin of this excess in ^{33}S, Rai et al. (2005) concluded that mass-independent induced gas phase chemical reactions in the solar nebula was more likely to explain positive $\Delta^{33}S$ up to 0.16 ‰ in Norton County. Though our results are distinct in sign and magnitude we confirm that oldhamite, or at least, the water soluble fraction, is a carrier of MIF. The contrast of 0.25 ‰ in $\Delta^{33}S$ between Rai et al. 2005 and this study could be the illustration of significant heterogeneity in the Norton County meteorite.

On Earth, photochemistry reactions between UV on S-atmospheric species, such as SO_2, leads to the production of MIF (Farquhar et al. 2000a, 2001). This is a well-accepted origin for terrestrial MIF recorded in Archean sulfides and sulfates as well as present-day sulfate aerosols in Antarctic ice cores (Baroni et al. 2007, 2008). One of the solar nebula prominent species in gas phase in reducing environment nebula is H_2S. The specific isotope fractionations associated with photodissociation of H_2S are still based on a very limited set of experiments at specific wavelengths. Experiments using a wavelength of ~220 nm show a positive $\Delta^{36}S/\Delta^{33}S$ ratio of ≈ +1.7 (Farquhar et al. 2000b) while Chakraborty et al. (2013) showed that using a Lyman-α radiation (121.6 nm), that was suggested to be more representative of a T-Tauri sun, the $\Delta^{36}S/\Delta^{33}S$ ratio becomes negative with a value of ≈ -3.

383 Though this result supports the MIF observed in iron meteorites by Antonelli et al. (2014), it
384 does not match our own results. It remains possible that at a particular wavelength, or a
385 distinct spectrum that might have existed during the early stage of the Solar Nebula,
386 photochemistry created a MIF with a much stiffer slope (a $\Delta^{36}S/\Delta^{33}S$ ratio of ≈ -12 would be
387 necessary to match our data and account for the $\Delta'^{33}S$ of -0.085 ‰ measured in Norton
388 County) but this remains to be produced by experimental data. Though the Lyman-α is the
389 strongest wavelength in the nebula, a contribution of other wavelengths, others sulfide
390 species (HS, SiS, etc…), or systems with different composition (e.g. dust/gas ratio) might lead
391 to a distinct MIF signal. Further studies are required to help clarify these issues.
392
393 S isotope anomalies associated with nucleosynthetic sources were recently reviewed by
394 Antonelli et al. (2014). Clayton and Ramadurai (1977) predicted an enrichment in ^{36}S while
395 enrichment in ^{32}S compared to the three other S isotopes was predicted by Farquhar et al.
396 (2000), with a slope of 1 in $\delta^{33}S$ vs. $\delta^{34}S$ and $\delta^{36}S$ vs. $\delta^{34}S$ diagrams, thus leading to a constant
397 ratio of $\Delta^{36}S/\Delta^{33}S \approx -1.9$. This was later confirmed by Hoppe et al. (2012), though ^{36}S was not
398 measured. Presolar SiC grains have indeed shown depletion in ^{33}S resulting in a $\Delta^{33}S$ as low
399 as -200 ‰. Those values are thought to be inherited from S formed in the Si/S zone of SNII
400 Supernovae (Hoppe et al. 2012). Nucleosynthetic processes in SNII supernovae could also
401 produce enrichments in ^{36}S (Woosley & Heger 2007), but those would be observed in the
402 He/C zone and are thought to be associated with an enrichment in ^{33}S, resulting in positive
403 $\Delta^{33}S$ and $\Delta^{36}S$. None of these match our data, neither the bulk fraction (that shows no
404 significant MIF, see Figure 2), nor in the water soluble fraction (Figure 4).
405

406 Antonelli et al. (2014) measured the S isotopic compositions of iron meteorite troilites. They
407 noted slight MIF, both positive and negative (-0.029 ‰ < $\Delta^{33}S$ < +0.031 ‰, -0.34 ‰ < $\Delta^{36}S$ <
408 +0.28 ‰), showing a weak correlation of $\Delta^{33}S/\ \Delta^{36}S \approx -7$ that they interpret as being the
409 produce of nebular photochemistry. Our data strongly overlap with those of Antonelli et al.
410 (2014) being, therefore, consistent with such a process. However, the more restricted ranges
411 in both $\Delta^{33}S$ and $\Delta^{36}S$ does not support the possibility of photochemistry-related isotope
412 effect in our data. None of the above hypotheses gives a trend that matches the observed
413 MIF in the water soluble fraction of the enstatite meteorite (Figure 4), and are thus unlikely
414 explanation for our set of data.
415
416 Alternatively, the excess of ^{36}S could be inherited from another water soluble phase that
417 would contaminate the water soluble fraction during chemical extraction of the oldhamite. If
418 a phase carrying an excess of ^{36}S were to contaminate the oldhamite extract, then this
419 excess could be misinterpreted as coming from the oldhamite itself. A possible candidate of
420 such contamination is lawrencite ($FeCl_2$). Indeed, lawrencite is water soluble and large
421 excesses (> 200 ‰) of $\Delta^{36}S$ have been measured and have been interpreted as the result of
422 the decay of $^{36}Cl \rightarrow {}^{36}S$ (½ life ≈ 301,000 ± 2,000 years) (Lin et al. 2005, Jacobsen et al. 2011).
423 ^{36}S is the rarest stable isotope of sulfur (~ 0.017%) and, as such, is the most sensitive to
424 secondary isotope production. ^{36}Cl (½ life ≈ 301,000 ± 2,000 years) decays in both ^{36}Ar and
425 ^{36}S (~ 99 and 1% respectively via $^{35}Cl(n, g)^{36}Cl \rightarrow {}^{36}Ar, {}^{36}S$) and given the bearing of noble gas
426 geochemistry to date exposure ages, ^{36}Cl-production has therefore been widely studied, and
427 is known to occur from several elements most primarily Fe, Ti, Ca and Cl (e.g. Leya et al.,
428 2000a, 2000b). ^{36}S production from ^{36}Cl-decay is a viable explanation to account for the
429 occurrence of positive $\Delta^{36}S$ in our sample set together with a lack of $\Delta^{33}S$-anomaly. The only

exception is, again, for Norton County. Other mechanisms such as spallation reactions on Fe (see above) would indeed lead to coupled $\Delta^{33}S$ and $\Delta^{36}S$-anomalies, which are not observed in our dataset. The fact that positive $\Delta^{36}S$ are measured in two aubrites (i.e. with lower Fe-contents than enstatite chondrites) is also consistent with such an observation.

Radioactive ^{36}Cl is commonly suggested to result from either nucleosynthetic anomalies (e.g. Murty et al. 1997), neutron capture reactions of Cl-rich fluid/phase for example during T-Tauri phase of the sun (Wasserburg et al. 2011, Jacobsen, 2011, Turner et al. 2013) and/or it subsequent production from primary and secondary particles on the parent body. Enstatite and aubrites have long exposure time (for review see Eugster, 2003), consistent with e.g. Sm and Gd isotopic studies (e.g. Hidaka et al., 2012).

Lawrencite ($FeCl_2$) was found to bear large excesses of ^{36}S ($\Delta^{36}S$ > 200 ‰) which were interpreted as the result of the decay of $^{36}Cl \rightarrow {}^{36}S$ (Lin et al. 2005, Jacobsen et al. 2011). Lawrencite is found in enstatite meteorites, for example it was described as an accessory mineral in the EL3 fragment of the polymict meteorite Almahata Sitta (Lin et al. 2011, Feng et al. 2012) and many other aubrites and chondrites (e.g. Lundberg et al., 1994). If produced by ^{36}Cl-decay produced from ^{35}Cl, $\Delta^{36}S$ anomalies should be coupled with enrichment in both ^{36}Ar and ^{38}Ar, the latter being produced from $^{37}Cl(n, g)^{38}Cl \rightarrow {}^{38}Ar$. Excesses of ^{36}Ar have been observed in several enstatite chondrites (Okazaki et al. 2010) and aubrites (Miura et al. 2006). Establishing relationships between ^{36}Ar and ^{38}Ar budgets remain however difficult to address. The respective contribution of initial 'trapped' and produced 'cosmogenic' Ar are notably hard to calculate and is further complicated by the sensitivity of argon isotopes to terrestrial weathering (Patzer and Schultz, 2001). However, we did not identify any

454 relationship between $\Delta^{36}S$ and exposure age (see Table 2). Although the lack of relationship
455 may be taken as an argument against $\Delta^{36}S$ anomalies resulting from ^{36}Cl-decay, it is worth
456 noting that exposure age of aubrites (i.e. 2 of our 3 samples yielding non-zero $\Delta^{36}S$) may be
457 biased, most data being obtained on brecciated samples (Wieler, 2002; Eugster 2003, p. 11).
458 Yet lawrencite ($FeCl_2$) is a water soluble mineral and it is a likely to react and released its
459 sulfur during the extraction of the water soluble fraction and, we suggest, is a possible
460 candidate that should deserve future investigations. The ^{36}S excess measured in the water
461 soluble fraction does not exceed 2 ‰. Assuming that this anomaly is entirely produced by
462 the excess of ^{36}S from lawrencite and that this original excess is of ≥200 ‰, mass balance
463 shows that less than 3 % of the ^{36}S from the water soluble fraction would come from the
464 contribution of lawrencite, which in turn represents ≈ 0.1 % of the total S in the samples.
465
466 It is also possible that the excess of $\Delta^{36}S$ measured in the water soluble fraction originates
467 from reactions with calcium, about half being likely contained in oldhamite. Few studies
468 were devoted to the specific analysis of oldhamite; so far, no significant isotope anomaly has
469 been recognized for Ca or S-isotopes (e.g. Lundberg et al., 1994). The errors on S-
470 measurements (typically 2-4‰) were however too large compared with the scale of $\Delta^{36}S$
471 anomalies we report. Therefore, we cannot exclude that the oldhamite is not the main
472 carrier of $\Delta^{36}S$-anomalies and future work on oldhamite could clarify this issue. Similarly,
473 such investigations could help understanding the origin of the very positive $\delta^{34}S$-values, up
474 to +11‰, measured in the water-soluble fraction.
475
476 The high reactivity of oldhamite and lawrencite with water could explain why it is only
477 observed in highly reduced meteorites such as enstatite chondrites and achondrites, as the

slightest contact with water (aqueous alteration, weathering, sample preparation) in C and O chondrites is likely to dissolve this mineral phase and mix it with the other sulfide/sulfate pool (Larimer 1968). Moreover, if the ^{36}S excess results from the decay of ^{36}Cl, it will have no effect on the bulk S isotopic compositions of the samples, which is consistent with the lack of correlation between $\Delta'^{33}S$ and $\Delta'^{36}S$.

4.3. Parent Bodies

Our data show that it is not possible to discriminate EH3, EH5 and EL3 from their isotopic composition of sulfur. Enstatite chondrites formed in an extremely reduced environment, with a fO_2 as low as 10^{-21} atm (800°C), significantly different from the environment of formation of ordinary and carbonaceous chondrites, that show a fO_2 respectively two and three order of magnitude higher (Brett & Sato, 1983). It is possible that it is these common and peculiar conditions of formations that led to similar isotopic compositions for EL and EH parent bodies, whatever EH and EL derive or not from the same parent body. Based upon the chemical compositions of enstatite chondrites, Kallemeyn and Wasson (1986) suggested that the innermost region of the solar nebula, where enstatite meteorites most probably formed, had to be heterogeneous. Gao and Thiemens (1993a) argued against this idea, based on the evidence that EH and EL had distinct parent bodies, and yet similar S and O isotopic composition. Therefore the inner region of the nebula had to be isotopically homogeneous. However, the recent discovery of a small but significant difference between EL ($\Delta^{17}O$ = -0.041 ± 0.026 ‰) and EH ($\Delta^{17}O$ = -0.066 ± 0.027 ‰) would rather favor a slightly heterogeneous nebula (Herwartz et al. 2014). Thus, if an S isotope heterogeneity exists

among EH and EL, it remains within our experimental error. However, our data showing that the EL6 (average $\delta^{34}S$ = -0.66 ± 0.14 ‰ while average EH: $\delta^{34}S$ = -0.25 ± 0.21 ‰) might have a distinct S composition, offers two possibilities. It can either indicate heterogeneities in the isotopic composition of sulfur in the inner area of the nebula, or the parent body processes that altered the original S composition of EL6/7. Yet, a difference between the Earth's mantle and ocean of 0.1 ‰ in $\Delta^{17}O$ (Pack and Herwartz 2013) is comparatively larger than the difference between EL and EH. If a mechanism can produce up to 0.1 ‰ on Earth, then we enter a field where a difference of 0.3 ‰ in $\delta^{34}S$ between EL and EH may not be significant enough to highlight a nebula heterogeneity, as processes on the parent body might alternatively lead to such variability.

Even though it is generally assumed that the EH and EL groups represent only two parent bodies, some recent studies have shown remarkable differences between EL6 and other enstatite chondrites (Rubin et al. 2009, Moynier et al. 2011, Barrat et al. 2014, Wang et al. 2014). In agreement with our results, showing that the sulfur isotopic ratio of EL6 is distinct from all the other enstatite chondrites, Moynier et al. (2011) have shown that the EL6 are depleted in Zn, with an estimated Zn concentration of 6 ppm (Kong et al. 1997) whereas EL3 show a Zn content of 213 ppm (Kong et al. 1997) and EH chondrites show a Zn content of 290 ppm (Lodders and Fegley 1998), and were also enriched in light Zn isotopes, showing a $\delta^{66}Zn$ = +4.88 ± 1.79 ‰ (1σ), compared to the other enstatite groups, both chondrites ($\delta^{66}Zn$ = +0.25 ± 0.16 ‰ (1σ)) and aubrites ($\delta^{66}Zn$ = +4.88 ± 1.79 ‰ (1σ)). Preferential loss of the heavier Zn isotopes would be caused by volatilization by impacts on the parent body of EL6. However, EL6 are enriched in light S isotopes, and not heavy S isotopes. Kinetically driven evaporation would enrich the residue in heavier S isotopes (e.g. Davis and Richter 2003), so

cannot explain the depletion in ^{34}S in EL of the highest metamorphic degree. One alternative explanation could be an oxidation occurring on the EL6 parent body. McEwing et al. (1983) showed that oxidation of FeS sulfides caused enrichment in heavy S isotopes of the residue. Being the most reduced bodies, an oxidation of enstatite chondrites would lead to marked petrographic features between EL6 and other enstatite meteorites, which is however not the case, making oxidation of EL6 an unlikely explanation. Oldhamite (which can be ^{34}S enriched) being one of the most refractory minerals, its preferential evaporation is also unlikely.

REE studies (Rubin et al. 2009, Barrat et al. 2014) and Fe isotopic compositions (Wang et al. 2014) have also shown a unique behaviour in EL6 compared to other enstatite meteorites. Rubin et al. (2009) reported that the EL6 are depleted in siderophile and chalcophile REE and that lithophile REE are more fractionated in EL6 than in other chondrites. For instance, in EL6, the ratio La/Yb = 0.79 against 1.05 for other enstatite chondrites (Rubin et al. 2009). The same goes for Sm/Yb (0.89 in EL6, 0.95 in EH), La/Sm (0.90 in EL6, 1.00 in EH) or Ca/Sc (0.86 in EL6, 0.97 in EH). They have also observed a depletion in the abundance of oldhamite in EL6, which is the main carrier of the REE along with plagioclase, that can account for the REE depletion and fractionation. Wang et al. (2014) measured the isotopic compositions of Fe in all groups of enstatite meteorites and noted that, in contrast with the homogeneous compositions of EH ($\delta^{56}Fe$ = 0.003 ± 0.042 ‰) and EL3 ($\delta^{56}Fe$ = 0.030 ± 0.038 ‰), the EL6 displayed a large variability in their Fe isotopic composition, showing a $\delta^{56}Fe$ varying from -0.180 ‰ to 0.181 ‰, which they explained as the consequences of the important brecciation underwent by EL6, mixing different proportions of mineral phases with distinct Fe isotopic compositions.

The petrographic grades determined for EH meteorites range from EH3 to EH5. Though EH6 do exist (Rubin & Wasson, 2011), very few have been studied. The EL group, on the other hand, shows a petrographic grade ranking up to EL6, and even EL7 for few samples. Happy Canyon is officially classified by the Meteoritical Bulletin Database as EL6/7 and Ilafegh 009 is classified as EL7. The petrographic grade of type 7 designates chondrites that have been metamorphised nearly to the point of melting. Though this term is not widely accepted, it undoubtedly indicates the highest degree of metamorphism possible for an undifferentiated body.

Thus, it is possible that the EL parent body underwent a stronger metamorphism than the EH parent body, and that this metamorphism has affected the S isotopic composition of metamorphosed material of the EL parent body while not impacting the isotopic composition of the EH parent body. Other chondritic groups do not evidence a similar difference between petrographic grades, but no study reports a complete set of petrographic grades in a particular group of meteorites and there are no high metamorphic grades in carbonaceous chondrites. However, Gao and Thiemens (1993a) measured the sulfur isotopic composition of several ordinary chondrites, including the L3 ALHA 77216 and the LL6 ALHA 83071 and no significant difference were observed compared with other OC meteorites of lower metamorphic grade.

All the compositional differences noted in EL6 compared to others enstatite meteorites can be explained by an impact-induced high metamorphism on a unique EL parent body, creating locally a volatilization of Zn (Moynier et al. 2011), a fractionation and depletion in REE (Rubin et al. 2011, Barrat et al. 2014), and the large brecciation, causing heterogeneity

574 of the Fe isotopic composition (Wang et al. 2014) as well as the loss of oldhamite that
575 produced the light isotopic composition in S (this study).
576
577 **4.4. Mass Dependent Isotopic Fractionation and loss of Oldhamite**
578
579 The variable $\delta^{34}S$ observed in the water soluble fraction (from 0.7 ‰ up to +10.95 ‰), is
580 distinctively different from the bulk isotopic composition that is homogeneous and slightly
581 and consistently negative in all enstatite meteorites. There are two ways to explain the
582 oldhamite ^{34}S isotopic compositions. These positive signatures are either pristine, in which
583 case it testifies of a different S reservoir for oldhamite than the other S-bearing minerals in
584 the enstatite meteorites, or it has been isotopically modified and reflects an alteration
585 process that affected only the (soluble) oldhamite. In the case of a pristine S isotopic
586 composition, oldhamite would be the testimony of the existence of yet unknown reservoir,
587 with the $\Delta^{33}S$ remaining unaffected by any of the MIF-inducing processes highlighted before
588 (spallation, UV photolysis, nucleosynthetic sources) with the possible exception of the
589 negative $\Delta^{33}S$ in Norton County.
590
591 Evaporation of CaS would lead to positive $\delta^{34}S$ of residual CaS and, according to mass
592 conservation effects (Farquhar et al., 2007) would also lead to significant but limited MIF:
593 modelling was made using fractionation factors scaling to the square root of the mass of the
594 evaporated species (Davies et al., 1990; Young et al., 2002) and shows that the maximum
595 $\Delta^{33}S$ and $\Delta^{36}S$ would be -0.04 and 0.26‰ respectively for a residual $\delta^{34}S$ of 10 ‰. Therefore,
596 evaporation cannot be the main process responsible for $\Delta^{36}S$ anomalies up to +2.2‰, even if

597 we cannot rule out that it might have contributed, among other processes, to the observed
598 isotope variability of oldhamite (or soluble fraction).
599
600 Alternatively, oldhamite is a mineral that has an extraordinary high melting temperature of
601 about 2525°C as a pure substance (McCoy et al. 1999) but can also melts at much lower
602 temperatures in conjunction with other phases, in particular, low fO_2 CaO-MgO-SiO_2-CaS
603 systems (Rudneva and Panov, 1962) and enstatite-chondrite melts (Fogel et al. 1996). Fusion
604 experiments on Indarch have shown that at 1000°C, all sulfides and metal phases were
605 melted (McCoy et al. 1999). This supports the idea that oldhamite should be lost through
606 metamorphism on the EL parent body, though the occurrence of oldhamite in aubrites
607 seems inconsistent with such an assumption.
608 It seems thus likely that a kinetic-driven alteration process could affect its S isotopic
609 composition, leading to high ^{34}S residual compositions of the oldhamite. Figure 5 shows that
610 apart from one anomalously CaS-rich sample (Indarch), a correlation seems to exist between
611 $\delta^{34}S$ of the oldhamite and its proportion in sulfides. This suggests that the loss of CaS
612 induced a concentration of heavy isotopes and thus higher $\delta^{34}S$ in the oldhamite residue,
613 either during impact-induced melting events on the parent body or on the Earth's surface
614 during subsequent storage.
615
616 At equilibrium, Cas is likely to be enriched by ~0.15 ‰ in ^{34}S, compared to FeS at T ≈ 1200°C
617 (as determined by extrapolating data from Ohmoto & Rye 1979; see Moretti et al. for
618 review), while this value would rise to ≈ 2.5 ‰ at T ≈ 200°C. The loss of oldhamite is
619 therefore consistent with a decrease of $\delta^{34}S$ of EL6/7 but the most positive $\delta^{34}S$ values are
620 inconsistent with equilibrium processes and may highlight low temperature kinetic effects.

Previous studies (Rubin et al. 2009, Barrat et al. 2014) have suggested that loss of oldhamite to account for differences in REE content between EL3 and EL6. Lower REE concentrations in EL6 than in EL3 showed that REE are lost along with the oldhamite during impact-induced melting on the parent body and probably redistributed to other parts of the parent body. In every analyzed samples, the oldhamite fraction (0 to 20 % of total sulfur) shows a distinctively ^{34}S enriched isotopic composition, and this ^{34}S enrichment can be used to quantify this possibility. Because of the absence of EL3 fall and the most likely loss of oldhamite due to terrestrial alteration of EL3 finds and the loss of oldhamite observed in EL6 it is impossible to quantify the original amount and isotopic composition of oldhamite on the EL6 parent body. However, since EH3, EH5 and aubrites do not show any systematic S isotopic variations we suggest that, despite the large variations observed of composition observed between the different groups, that they are the best available proxy to estimate the isotopic composition of the EL parent body.

In order to estimate the loss of oldhamite between EL3 and EL6, we need to estimate the $\delta^{34}S$ of the non-soluble (non-oldhamite) fraction. We make the hypothesis that the most ^{34}S-depleted composition measured in an enstatite chondrite (in Pillistfer) corresponds to a 100% loss of oldhamite, and therefore, a *non-soluble* value: $\delta^{34}S_{\text{non soluble}}$ = -1.17 ± 0.01 ‰. Keeping in mind that Pillistfer may contain trace amounts of CaS, this value must be taken as an upper estimate of the *non-soluble* value. The mass balance for EL3 can be written:

$$\delta^{34}S_{\text{total}}\ (\text{EL3}) = X \,.\, \delta^{34}S_{\text{non soluble}} + (1\text{-}X) \,.\, \delta^{34}S_{\text{CaS}} \qquad (3)$$

with X the fraction of non-soluble sulfides and $\delta^{34}S_{\text{total}}$ (EL3) = -0.32 ± 0.15 ‰.

With Y the fraction of CaS lost, the mass balance for EL6 becomes:

$$\delta^{34}S_{total}\ (EL6) = X\ .\ \delta^{34}S_{non\ soluble} + (1\text{-}X)(1\text{-}Y)\ .\ \delta^{34}S_{CaS} \qquad (4)$$

Assuming an average difference between EL3 and EL6 of 0.3 ‰, the fraction of oldhamite lost (Y) can be deduced as a function of $\delta^{34}S_{CaS}$ and X. We calculated X and Y for a large range of $\delta^{34}S_{CaS}$ from 0 to 11 ‰. We found that Y is little sensitive to $\delta^{34}S_{CaS}$ with most values between 50 and 36 % for a range of $\delta^{34}S_{CaS}$ between 2.2 and 10.9 ‰ and corresponding X varying between 25 and 7 % respectively. This is slightly lower than Rubin et al. (2009)'s 60 % estimate of the loss of oldhamite, though remains consistent with the idea that the loss of oldhamite is linked to a difference in ^{34}S between EL3 and EL6.

Therefore it does not seem necessary to invoke a distinct parent body to explain the difference of composition of EL6 compared to EL3. An advanced metamorphism, leading to the loss of oldhamite, which melts at relatively low temperatures and migrates to other regions of the parent body, can easily explain the S isotopic composition of EL6, as well as differences in composition in REE. Metamorphism and loss of oldhamite would likely be induced by impacts on the EL parent body, causing local heating, which is also supported by the loss of heavy Zn by impact-induced volatilization (Moynier et al. 2011).

4.5. The case of aubrites

Contrary to enstatite chondrites, aubrites display a very heterogeneous sulfur isotopic composition, showing the most extremes bulk values (-1.350‰ <$\delta^{34}S$< +0.154 ‰), including

669 intermediate values overlapping the chondritic values measured in their undifferenciated
670 counterparts. It is well accepted that the parent body of aubrites underwent local impact-
671 induced melting events, leading, at least locally, to segregation of the molten metal and
672 therefore partial differentiation. Segregation of metal and silicates causes a fractionation in S,
673 enriching the silicate phase in the lighter isotopes and the metallic phase in the heavier
674 isotopes (Shahar et al. 2009, Labidi et al. 2013). Aubrites are breccias, heavily rearranged
675 rocks. It is therefore highly probable that the large variations in the S isotopic compositions
676 reflect the various degrees of differentiations caused by the impact events and mixing with
677 impact-related compounds. Even the largest samples (~1 cm^3) remained relatively small
678 compared to the coarsed brecciation of aubrite meteorites of several cm wide, and
679 therefore were not representative of the bulk value of the meteorite samples. In particular,
680 this likely explains the variability observed in two distinct samples of Bishopville collected
681 from two different museum collections. In addition to the previously mentioned depletion in
682 heavy isotopes in relation of oldhamite loss, the most negative $\delta^{34}S$ values represents the S
683 composition of the most differentiated fraction of silicates. All together, these processes
684 likely explain the large S isotope variability of aubrites compared with other enstatite
685 meteorites.
686
687 **4.6. Comparison with the Earth and other meteorite groups**
688
689 Isotopic compositions of sulfur, and many other volatile and moderately-volatile elements (O,
690 Zn…), in enstatite meteorites and Earth have emphasized a number of similarities which led
691 to infer that they share a similar origin (Clayton et al. 1984, Javoy 1998, Javoy et al. 2010).
692 The Earth is depleted in volatile elements compared to primitive CI chondritic and enstatite

693 chondrites. It is possible that both the Earth and the Moon were essentially dry immediately
694 after the giant impact at the origin of the Moon and that most volatiles accreted later, as a
695 late veneer from e.g. carbonaceous chondrite or cometary-type material (Javoy 1998,
696 Albarède et al. 2013, Paniello et al. 2013). For volatile and chalcophile/siderophile elements
697 (Allègre et al. 1995, Malavergne et al. 2007, Dasgupta & Walker 2008, Wood and Halliday
698 2010, Wood et al. 2010), core segregation adds an additional level of complexity.
699
700 In meteorites, sulfur is usually described as "chondritic" reflecting a limited isotope
701 variability. The different meteorite groups and each class of meteorite greatly overlap, yet
702 they have a rather narrow and distinct range of variation (Gao & Thiemens 1993a, Gao &
703 Thiemens 1993b). Enstatite meteorites (average $\delta^{34}S$ = -0.47 ± 0.44 ‰ (1σ)) are enriched in
704 lighter isotopes compared to both ordinary chondrites (average $\delta^{34}S$ = 0.04 ± 0.38 ‰ (1σ),
705 Gao & Thiemens 1993a) and carbonaceous chondrites. Carbonaceous chondrites display the
706 largest range, exceeding all the measured compositions in other meteorites, with sulfides
707 enriched in heavy isotopes (average $\delta^{34}S$ = 2.02 ± 1.01 ‰ (1σ) Gao & Thiemens 1993b)
708 compared to other meteoritic groups, while sulfates (average $\delta^{34}S$ = -0.48 ± 1.01 ‰ (1σ) Gao
709 & Thiemens 1993b) display particularly ^{34}S-depleted isotope compositions, most likely
710 representing secondary products formed during aqueous alteration of the carbonaceous
711 chondrite parent body (Gao and Thiemens 1993b) or appeared after their fall on Earth
712 (Gounelle & Zolenski 2001). Early studies thus suggested that the original sulfur composition
713 of the CC parent body was actually enriched in heavy isotopes, though this has been
714 disproved more recently by Bullock et al. (2010).
715

It so appears that the enstatite meteorites are the closest class of meteorites to Bulk Silicate Earth (BSE) in terms of S isotopes. Labidi et al. (2013) recently re-investigated the isotopic compositions of the convective mantle through the study of mid-ocean ridge basalts. Even though a certain variability has been observed in the isotopic composition of modern hotspots (Cabral et al. 2013), implying a variability preserved in the convective mantle, the continental crust and sediments bear reasonably little sulfur to change significantly the global budget. The convective mantle is thus representative of the BSE being comprised between -1.80 ‰ and -1.05 ‰, with an average estimate of -1.28 ± 0.33 ‰. Assuming a chondritic Earth of -0.02 ± 0.06 ‰ in $\delta^{34}S$ (Gao and Thiemens 1993b), and about 97% of terrestrial sulfur stored in the core (Dreibus and Palme (1996), the isotope composition of BSE is compatible with a core being enriched in ^{34}S compared with the residual mantle. They inferred a core-mantle isotopic fractionation factor for the $^{34}S/^{32}S$ ratio of $\alpha_{core\text{-}mantle}$ = 1.00130 (Labidi et al. 2013) compatible with the value experimentally determined by Shahar et al. (2009). This estimate is dependent on the amount of sulfur brought to Earth by late accretion events, such as the late veneer, occurring after the core segregation, which was neglected. If the little variability of "chondritic" S in meteorites (i.e. similar to OC and CC) rules out late veneer as the main contribution to the mantle, in the details, however, meteorites display a significant range of values.

The enrichment in light isotopes measured in EL6/7 as well as in aubrites, falls in the range of values reported by Labidi et al. (2013), suggesting that melting and differentiation could indeed lead to a silicate residual mantle depleted in ^{34}S. According to models (Javoy et al. 2010), since Earth accreted from enstatite-like material, a $\delta^{34}S$-depleted starting material can be inferred. Our data also show that the most primitive EC give an average $\delta^{34}S$ around –0.3 ‰, which is significantly different from the $\delta^{34}S \approx 0$ ‰ otherwise used, which therefore

changes the mass balance equation and requires re-estimating the amount of sulfur stored in the core. Assuming that the estimated isotopic fractionation factor remains the same ($\alpha_{core\text{-}mantle}$ = 1.00130), if the starting material is set at – 0.3 ‰, mass balance calculation shows that the amount of sulfur stored in the core drops to 75 %.

5. CONCLUSION

We measured the bulk S isotopic compositions of 33 enstatite meteorites (chondrites and aubrites) as well as the oldhamite fraction of 9 samples. As reported previously, enstatite chondrites have lighter isotopic compositions than other chondrites, displaying negative $\delta^{34}S$ in all but one samples. However, in contrast with Gao and Thiemens (1993), we showed that EL6 have a distinct S isotopic composition, even more enriched in light isotopes than all other enstatite chondrite groups. This is explained by a loss in oldhamite, which is ^{34}S-enriched. Aubrites show very variable S compositions, displaying the most extreme values. This is probably due to their brecciatic nature of impact-induced differentiated material and/or segregation of metal. MIF have been observed only in the oldhamite fraction and they are likely to be the product of an excess of ^{36}S produced by the decay of ^{36}Cl from $FeCl_2$, which probably contaminated the oldhamite (water soluble) fraction during its chemical extraction. The sulfur isotopic composition measured in enstatite chondrites is distinct from the Bulk Silicate Earth, yet EL6/7 and aubrites are approaching its isotopic composition, making, in all cases, the enstatite meteorites the closest to the Earth composition, and reinforcing the idea that Earth was built from enstatite-like material.

ACKNOWLEDGEMENTS

The samples analyzed during the course of this study were kindly provided by Muséum National d'Histoire Naturelle (France), the Université Pierre et Marie Curie (France), The Smithsonian Institute (USA), The Natural History Museum of London (UK), Hawai'i Institute of Geophysics and Planetology (USA), and the NASA meteorite working group. US Antarctic meteorite samples are recovered by the Antarctic search for Meteorites (ANSMET) program which has been funded by NSF and NASA, and characterized and curated in the department of Mineral Sciences of the Smithsonian Institution and Astromaterials Curation Office at NASA Johnson Space Center. The authors thank INSU and CNES for the PNP grant. FM thanks the ERC for the Pristine Starting Grant, the Institut Universitaire de France and the ANR for a chaire de recherche IDEX SPC.

REFERENCES

Albarede, F., Ballhaus, C., Blichert-Toft, J., Lee, C.-T., Marty, B., Moynier, F., Yin, Q.-Z. (2013) Asteroidal impacts and the origin of terrestrial and lunar volatiles. *Icarus* **222**, 44–52.

Allègre, C.J., Manhès, G., Göpel, C. (1995) The age of the Earth. *Geochim. Cosmochim. Acta* **59**, 1445–1456.

787 Antonelli, M.A., Kim, S.-T., Peters, M., Labidi, J., Cartigny, P., Walker, R.J., Lyons, J.R., Hoek, J.,
788 Farquhar, J. (2014) Early inner solar system origin for anomalous sulfur isotopes in
789 differentiated protoplanets. *Proc. Natl. Acad. Sci.* **111**, 17749–17754.
790 Baroni, M., Savarino, J., Cole-Dai, J., Rai, V.K., Thiemens, M.H. (2008) Anomalous sulfur isotope
791 compositions of volcanic sulfate over the last millennium in Antarctic ice cores. *J. Geophys.*
792 *Res. Atmospheres* **113**, D20112.
793 Baroni, M., Thiemens, M.H., Delmas, R.J., Savarino, J. (2007) Mass-Independent Sulfur Isotopic
794 Compositions in Stratospheric Volcanic Eruptions. *Science* **315**, 84–87.
795 Barrat, J.A., Zanda, B., Jambon, A., Bollinger, C. (2014) The lithophile trace elements in enstatite
796 chondrites. *Geochim. Cosmochim. Acta* **128**, 71–94.
797 Birck, J.L., Rotaru, M., Allègre, C.J. (1999) ^{53}Mn-^{53}Cr evolution of the early solar system. *Geochim.*
798 *Cosmochim. Acta* **63**, 4111–4117.
799 Brett, R., Keil, K. (1986) Enstatite chondrites and enstatite achondrites (aubrites) were not derived
800 from the same parent body. *Earth Planet. Sci. Lett.* **81**, 1–6.
801 Brett, R., Sato, M. (1984) Intrinsic oxygen fugacity measurements on seven chondrites, a pallasite,
802 and a tektite and the redox state of meteorite parent bodies. *Geochim. Cosmochim. Acta* **48**,
803 111–120.
804 Bullock, E.S., McKeegan, K.D., Gounelle, M., Grady, M.M., Russell, S.S. (2010) Sulfur isotopic
805 composition of Fe-Ni sulfide grains in CI and CM carbonaceous chondrites. *Meteorit. Planet.*
806 *Sci.* **45**, 885–898.
807 Cabral, R.A., Jackson, M.G., Rose-Koga, E.F., Koga, K.T., Whitehouse, M.J., Antonelli, M.A., Farquhar,
808 J., Day, J.M.D., Hauri, E.H. (2013) Anomalous sulphur isotopes in plume lavas reveal deep
809 mantle storage of Archaean crust. *Nature* **496**, 490–493.
810 Canfield, D.E., Raiswell, R., Westrich, J.T., Reaves, C.M., Berner, R.A. (1986) The use of chromium
811 reduction in the analysis of reduced inorganic sulfur in sediments and shales. *Chem. Geol.* **54**,
812 149–155.

Cartigny, P., Boyd, S., Harris, J., Javoy, M. (1997) Nitrogen isotopes in peridotitic diamonds from Fuxian, China: the mantle signature. *Terra Nova* **9**, 175–179.

Casanova, I., Keil, K., Newsom, H.E.,(1993) Composition of metal in aubrites: Constraints on core formation. *Geochim. Cosmochim. Acta* **57**, 675–682.

Chakraborty, S., Jackson, T.L., Ahmed, M., Thiemens, M.H. (2013) Sulfur isotopic fractionation in vacuum UV photodissociation of hydrogen sulfide and its potential relevance to meteorite analysis. *Proc. Natl. Acad. Sci.* **110**, 17650–17655.

Clayton, D.D., Ramadurai, S. (1977) On presolar meteoritic sulphides. *Nature* **265**, 427–428

Clayton, R.N., Mayeda, T.K. (1996) Oxygen isotope studies of achondrites. *Geochim. Cosmochim. Acta* **60**, 1999–2017.

Clayton, R.N., Mayeda, T.K., Rubin, A.E. (1984) Oxygen isotopic compositions of enstatite chondrites and aubrites. *J. Geophys. Res. Solid Earth* **89**, C245–C249.

Dasgupta, R., Walker, D. (2008) Carbon solubility in core melts in a shallow magma ocean environment and distribution of carbon between the Earth's core and the mantle. *Geochim. Cosmochim. Acta* **72**, 4627–4641.

Dauphas, N., Davis, A.M., Marty, B., Reisberg, L. (2004) The cosmic molybdenum–ruthenium isotope correlation. *Earth Planet. Sci. Lett.* **226**, 465–475.

Davis, A.M., Richter, F.M. (2007) Condensation and Evaporation of Solar System Materials, *Treatise on Geochemistry*, pp. 1–31.

Dreibus, G., Palme, H. (1996) Cosmochemical constraints on the sulfur content in the Earth's core. *Geochim. Cosmochim. Acta* **60**, 1125–1130.

El Goresy, A., Yabuki, H., Ehlers, K., Woolum, D., Pernicka, E. (1988) Qingzhen and Yamato-691: A tentative alphabet for the EH chondrites. *Antarct. Meteor. Res.* **1**, 65.

Eugster, O., 2003. Cosmic-ray exposure ages of meteorites and lunar rocks and their significance. *Chemie Der Erde-Geochemistry* **63**, 3-30.

838 Farquhar, J., Jackson, T.L., Thiemens, M.H. (2000a) A 33S enrichment in ureilite meteorites: evidence
839 for a nebular sulfur component. *Geochim. Cosmochim. Acta* **64**, 1819–1825.
840 Farquhar, J., Savarino, J., Jackson, T.L., Thiemens, M.H. (2000b) Evidence of atmospheric sulphur in
841 the martian regolith from sulphur isotopes in meteorites. *Nature* **404**, 50–52.
842 Farquhar, J., Savarino, J., Airieau, S., Thiemens, M.H. (2001) Observation of wavelength-sensitive
843 mass-independent sulfur isotope effects during SO_2 photolysis: Implications for the early
844 atmosphere. *J. Geophys. Res. Planets* **106**, 32829–32839.
845 Feng, L., Elgoresy, A., Zhang, J., Hao, J., Boyet, M., Yang, L. (2012) Excess ^{36}S in Lawrencite and
846 Nitrogen Isotopic Compositions of Sinoite from Almahata Sitta MS-17 EL3 Chondrite
847 Fragment. *Lunar and Planetary Science Conference*, p. 1766.
848 Fitoussi, C., Bourdon, B. (2012) Silicon Isotope Evidence Against an Enstatite Chondrite Earth. *Science*
849 **335**, 1477–1480.
850 Gao, X., Thiemens, M.H. (1991) Systematic study of sulfur isotopic composition in iron meteorites
851 and the occurrence of excess ^{33}S and ^{36}S. *Geochim. Cosmochim. Acta* **55**, 2671–2679.
852 Gao, X., Thiemens, M.H. (1993a) Variations of the isotopic composition of sulfur in enstatite and
853 ordinary chondrites. *Geochim. Cosmochim. Acta* **57**, 3171–3176.
854 Gao, X., Thiemens, M.H. (1993b) Isotopic composition and concentration of sulfur in carbonaceous
855 chondrites. *Geochim. Cosmochim. Acta* **57**, 3159–3169.
856 Gounelle, M., Zolensky, M.E. (2001) A terrestrial origin for sulfate veins in CI1 chondrites. *Meteorit.*
857 *Planet. Sci.* **36**, 1321–1329.
858 Herwartz, D., Pack, A., Friedrichs, B., Bischoff, A. (2014) Identification of the giant impactor Theia in
859 lunar rocks. *Science* **344**, 1146–1150.
860 Hidaka, H., Kondo, T., and Yoneda, S., 2012. Heterogeneous isotopic anomalies of Sm and Gd in the
861 Norton County meteorite: evidence for irradiation from the active early sun. *Astrophysical*
862 *Journal* **746**.

Hoppe, P., Fujiya, W., Zinner, E. (2012) Sulfur Molecule Chemistry in Supernova Ejecta Recorded by Silicon Carbide Stardust. *Astrophys. J. Lett.* **745**, L26.

Hulston, J.R., Thode, H.G. (1965a) Cosmic-ray-produced S36 and S33 in the metallic phase of iron meteorites. *J. Geophys. Res*. **70**, 4435–4442.

Hulston, J.R., Thode, H.G. (1965b) Variations in the ^{33}S, ^{34}S, and ^{36}S contents of meteorites and their relation to chemical and nuclear effects. *J. Geophys. Res.* **70**, 3475–3484.

Jacobsen, B., Matzel, J., Hutcheon, I.D., Krot, A.N., Yin, Q.-Z., Nagashima, K., Ramon, E.C., Weber, P.K., Ishii, H.A., Ciesla, F.J. (2011) Formation of the short-lived radionuclide ^{36}Cl in the protoplanetary disk during late-stage irradiation of a volatile-rich reservoir. *Astrophys. J. Lett.* **731**, L28.

Javoy, M. (1998) The birth of the Earth's atmosphere: the behaviour and fate of its major elements. *Chem. Geol.* **147**, 11–25.

Javoy, M., Kaminski, E., Guyot, F., Andrault, D., Sanloup, C., Moreira, M., Labrosse, S., Jambon, A., Agrinier, P., Davaille, A., others(2010) The chemical composition of the Earth: Enstatite chondrite models. *Earth Planet. Sci. Lett.* **293**, 259–268.

Javoy, M., Pineau, F. (1983) Stable isotope constraints on a model Earth from a study of mantle nitrogen. *Meteoritics* **18**, 320.

Johnston, D.T., Farquhar, J., Habicht, K.S., Canfield, D.E. (2008) Sulphur isotopes and the search for life: strategies for identifying sulphur metabolisms in the rock record and beyond. *Geobiology* **6**, 425–435.

Kallemeyn, G.W., Wasson, J.T. (1986) Compositions of enstatite (EH3, EH4,5 and EL6) chondrites: Implications regarding their formation. *Geochim. Cosmochim. Acta* **50**, 2153–2164.

Keil, K. (1968) Mineralogical and chemical relationships among enstatite chondrites. *J. Geophys. Res.* **73,** 6945–6976.

Keil, K. (2010) Enstatite achondrite meteorites (aubrites) and the histories of their asteroidal parent bodies. *Chem. Erde - Geochem.* **70**, 295–317.

889 Kong, P., Mori, T., Ebihara, M. (1997) Compositional continuity of enstatite chondrites and
890 implications for heterogeneous accretion of the enstatite chondrite parent body. *Geochim.*
891 *Cosmochim. Acta* **61**, 4895–4914.
892 Labidi, J., Cartigny, P., Birck, J.L., Assayag, N., Bourrand, J.J. (2012) Determination of multiple sulfur
893 isotopes in glasses: A reappraisal of the MORB $\delta^{34}S$. *Chem. Geol.* **334**, 189–198.
894 Labidi, J., Cartigny, P., Moreira, M. (2013) Non-chondritic sulphur isotope composition of the
895 terrestrial mantle. *Nature* **501**, 208–211.
896 Larimer, J.W. (1968) An experimental investigation of oldhamite, CaS; and the petrologic significance
897 of oldhamite in meteorites. *Geochim. Cosmochim. Acta* **32**, 965–982.
898 Leya, I., Lange, H. J., Lupke, M., Neupert, U., Daunke, R., Fanenbruck, O., Michel, R., Rosel, R.,
899 Meltzow, B., Schiekel, T., Sudbrock, F., Herpers, U., Filges, D., Bonani, G., Dittrich-Hannen, B.,
900 Suter, M., Kubik, P. W., and Synal, H. A., 2000a. Simulation of the interaction of galactic
901 cosmic-ray protons with meteoroids: On the production of radionuclides in thick gabbro and
902 iron targets irradiated isotropically with 1.6 GeV protons. *Meteoritics & Planetary Science* **35**,
903 287-318.
904 Leya, I., Lange, H. J., Neumann, S., Wieler, R., and Michel, R., 2000b. The production of cosmogenic
905 nuclides in stony meteoroids by galactic cosmic-ray particles. *Meteoritics & Planetary Science*
906 **35**, 259-286.
907 Leya, I. and Masarik, J., 2009. Cosmogenic nuclides in stony meteorites revisited. *Meteoritics &*
908 *Planetary Science* **44**, 1061-1086.
909 Lin, Y., El Goresy, A. (2002) A comparative study of opaque phases in Qingzhen (EH3) and MacAlpine
910 Hills 88136 (EL3): Representatives of EH and EL parent bodies. *Meteorit. Planet. Sci.* **37**, 577–
911 599.
912 Lin, Y., Guan, Y., Leshin, L.A., Ouyang, Z., Wang, D. (2005) Short-lived chlorine-36 in a Ca- and Al-rich
913 inclusion from the Ningqiang carbonaceous chondrite. *Proc. Natl. Acad. Sci.* **102**, 1306–1311.

914 Lin, Y., El Goresy, A., Boyet, M., Feng, L., Zhang, J., Hao, J. (2011) Earliest solid condensates consisting
915 of the assemblage oldhamite, sinoite, graphite and excess ^{36}S in lawrencite from Almahata
916 Sitta MS-17 EL3 Chondrite Fragment, *Workshop on Formation of the First Solids in the Solar*
917 *System*.
918 Lodders, K., Fegley, B. (1998) The planetary scientist's companion. *Oxford University Press*.
919 Lorenzetti, S., Eugster, O., Busemann, H., Marti, K., Burbine, T.H., McCoy, T. (2003) History and origin
920 of aubrites. *Geochim. Cosmochim. Acta* **67**, 557–571.
921 Lundberg, L. L., Zinner, E., and Crozaz, G., 1994. Search for isotopic anomalies in oldhamite (CaS) from
922 unequilibrated (E3) enstatite chondrites. *Meteoritics* **29**, 384-393.
923 Malavergne, V., Tarrida, M., Combes, R., Bureau, H., Jones, J., Schwandt, C. (2007) New high-pressure
924 and high-temperature metal/silicate partitioning of U and Pb: Implications for the cores of
925 the Earth and Mars. *Geochim. Cosmochim. Acta* **71**, 2637–2655.
926 Marini, L., Moretti, R., Accornero, M. (2011) Sulfur Isotopes in Magmatic-Hydrothermal Systems,
927 Melts, and Magmas. *Rev. Mineral. Geochem.* **73**, 423–492.
928 Mason, B. (1966) The enstatite chondrites. *Geochim. Cosmochim. Acta* **30**, 23–39.
929 McCoy, T.J., Dickinson, T.L., Lofgren, G.E. (1999) Partial melting of the Indarch (EH4) meteorite: A
930 textural, chemical, and phase relations view of melting and melt migration. *Meteorit. Planet.*
931 *Sci.* **34**, 735–746.
932 McEwing, C. e., Rees, C. e., Thode, H. g. (1983) Sulphur Isotope Ratios in the Canyon Diablo Metallic
933 Spheroids. *Meteoritics* **18**, 171–178.
934 Miura, Y.N., Hidaka, H., Nishiizumi, K., Kusakabe, M. (2007) Noble gas and oxygen isotope studies of
935 aubrites: A clue to origin and histories. *Geochim. Cosmochim. Acta* **71**, 251–270.
936 Moynier, F., Agranier, A., Hezel, D.C., Bouvier, A. (2010) Sr stable isotope composition of Earth, the
937 Moon, Mars, Vesta and meteorites. *Earth Planet. Sci. Lett.* **300**, 359–366.

938 Moynier, F., Day, J.M.D., Okui, W., Yokoyama, T., Bouvier, A., Walker, R.J., Podosek, F.A. (2012)
939 Planetary-Scale Strontium Isotopic Heterogeneity and the Age of Volatile Depletion of Early
940 Solar System Materials. *Astrophys. J.* **758**, 45.
941 Moynier, F., Paniello, R.C., Gounelle, M., Albarède, F., Beck, P., Podosek, F., Zanda, B. (2011) Nature
942 of volatile depletion and genetic relationships in enstatite chondrites and aubrites inferred
943 from Zn isotopes. *Geochim. Cosmochim. Acta* **75**, 297–307.
944 Newton, J., Franchi, I.A., Pillinger, C.T. (2000) The oxygen-isotopic record in enstatite meteorites.
945 *Meteorit. Planet. Sci.* **35**, 689–698.
946 Ohmoto, H., Rye, R. (1979) Isotopes of sulfur and carbon. Geochem. *Hydrothermal Ore Depos. Ed*
947 509–567.
948 Okazaki, R., Takaoka, N., Nagao, K., Nakamura, T., 2010. Noble gases in enstatite chondrites released
949 by stepped crushing and heating. *Meteorit. Planet. Sci.* **45**, 339–360.
950 Ono, S., Wing, B., Johnston, D., Farquhar, J., Rumble, D. (2006) Mass-dependent fractionation of
951 quadruple stable sulfur isotope system as a new tracer of sulfur biogeochemical cycles.
952 *Geochim. Cosmochim. Acta* **70**, 2238–2252.
953 Paniello, R.C., Day, J.M.D., Moynier, F. (2012) Zinc isotopic evidence for the origin of the Moon.
954 *Nature* **490**, 376–379.
955 Patzer, A., Schultz, L. (2001) Noble gases in enstatite chondrites I: Exposure ages, pairing, and
956 weathering effects. *Meteorit. Planet. Sci.* **36**, 947–961.
957 Quirico, E., Bourot-denise, M., Robin, C., Montagnac, G., Beck, P. (2011) A reappraisal of the
958 metamorphic history of EH3 and EL3 enstatite chondrites. *Geochim. Cosmochim. Acta* **75**,
959 3088–3102.
960 Rai, V.K., Jackson, T.L., Thiemens, M.H. (2005) Photochemical mass-independent sulfur isotopes in
961 achondritic meteorites. *Science* **309**, 1062–1065.

962 Robinson, B. W. (1995). Sulphur isotope standards. *Reference and intercomparison materials for*
963 *stable isotopes of light elements. IAEA-TECDOC-825. International Atomic Energy Agency,*
964 *Vienna*, 39K-45.
965 Rubin, A.E. (1984) The Blithfield meteorite and the origin of sulfide-rich, metal-poor clasts and
966 inclusions in brecciated enstatite chondrites. *Earth Planet. Sci. Lett.* **67**, 273–283.
967 Rubin, A.E., Huber, H., Wasson, J.T. (2009) Possible impact-induced refractory-lithophile
968 fractionations in EL chondrites. *Geochim. Cosmochim. Acta* **73**, 1523–1537.
969 Rubin, A.E., Wasson, J.T. (2011) Shock effects in "EH6" enstatite chondrites and implications for
970 collisional heating of the EH and EL parent asteroids. *Geochim. Cosmochim. Acta* **75**, 3757–
971 3780.
972 Rudneva, A.V., Panov, A.S. (1962) The effect of calcium sulfide on the phase composition of slags in
973 the system CaO-MgO-SiO2. *Bull. Acad. Sci. USSR Div. Chem. Sci.* **11**, 510–513.
974 Sanloup, C., Jambon, A., Gillet, P. (1999) A simple chondritic model of Mars. *Phys. Earth Planet. Inter.*
975 **112**, 43–54.
976 Savage, P.S., Moynier, F. (2013) Silicon isotopic variation in enstatite meteorites: Clues to their origin
977 and Earth-forming material. *Earth Planet. Sci. Lett.* **361**, 487–496.
978 Sears, D.W. (1980) Formation of E chondrites and aubrites—A thermodynamic model. *Icarus* **43**,
979 184–202.
980 Shahar, A., Fei, Y., Liu, M.C., Wang, J. (2009) Sulfur isotopic fractionation during the differentiation of
981 Mars. *Geochim. Cosmochim. Acta Suppl*. **73**, 1201.
982 Simon, J.I., DePaolo, D.J. (2010) Stable calcium isotopic composition of meteorites and rocky planets.
983 *Earth Planet. Sci. Lett.* **289**, 457–466.
984 Thode, H.G., Monster, J., Dunford, H.B. (1961) Sulphur isotope geochemistry. *Geochim. Cosmochim.*
985 *Acta* **25**, 159–174.
986 Trinquier, A., Birck, J.-L., Allègre, C.J. (2007a) Widespread 54Cr Heterogeneity in the Inner Solar
987 System. *Astrophys. J.* **655**, 1179.

988 Trinquier, A., Bizzarro, M., Ulfbeck, D. (2007b) 50 Ti anomalies in primitive and differentiated
989 meteorites. *Geochim Cosmochim Acta* **71**, A1038.
990 Trinquier, A., Elliott, T., Ulfbeck, D., Coath, C., Krot, A.N., Bizzarro, M. (2009) Origin of
991 Nucleosynthetic Isotope Heterogeneity in the Solar Protoplanetary Disk. *Science* **324**, 374–
992 376.
993 Turner, G., Crowther, S.A., Burgess, R., Gilmour, J.D., Kelley, S.P., Wasserburg, G.J. (2013) Short lived
994 36Cl and its decay products 36Ar and 36S in the early solar system. *Geochim. Cosmochim.*
995 *Acta* **123**, 358–367.
996 Valdes, M.C., Moreira, M., Foriel, J., Moynier, F. (2014) The nature of Earth's building blocks as
997 revealed by calcium isotopes. *Earth Planet. Sci. Lett.* **394**, 135–145.
998 Wang, K., Savage, P.S., Moynier, F. (2014) The iron isotope composition of enstatite meteorites:
999 Implications for their origin and the metal/sulfide Fe isotopic fractionation factor. *Geochim.*
1000 *Cosmochim. Acta* **142**, 149–165.
1001 Wasserburg, G.J., Hutcheon, I.D., Aléon, J., Ramon, E.C., Krot, A.N., Nagashima, K., Brearley, A.J.
1002 (2011) Extremely Na- and Cl-rich chondrule from the CV3 carbonaceous chondrite Allende.
1003 *Geochim. Cosmochim. Acta* **75**, 4752–4770.
1004 Watters, T.R., Prinz, M. (1979) Aubrites-Their origin and relationship to enstatite chondrites, *Lunar*
1005 *and Planetary Science Conference Proceedings*. pp. 1073–1093.
1006 Weisberg, M.K., Kimura, M. (2012) The unequilibrated enstatite chondrites. *Chem. Erde-Geochem.***72**,
1007 2, 101-115.
1008 Wieler, R., 2002. Cosmic-ray-produced noble gases in meteorites, *Noble Gases in Geochemistry and*
1009 *Cosmochemistry*. Rev. Mineral. Geo. **47**, 125-170.
1010 Wood, B.J., Halliday, A.N. (2010) The lead isotopic age of the Earth can be explained by core
1011 formation alone. *Nature* **465**, 767–770.
1012 Wood, B.J., Halliday, A.N., Rehkämper, M. (2010) Volatile accretion history of the Earth. *Nature* **467**,
1013 E6–E7.

Woosley, S.E., Heger, A. (2007) Nucleosynthesis and remnants in massive stars of solar metallicity. *Phys. Rep.* **442**, 269–283.

Zhang, J., Dauphas, N., Davis, A.M., Leya, I., Fedkin, A. (2012) The proto-Earth as a significant source of lunar material. *Nat. Geosci.* **5**, 251–255.

Zhang, Y., Benoit, P.H., Sears, D.W.G. (1995) The classification and complex thermal history of the enstatite chondrites. *J. Geophys. Res. Planets* **100**, 9417–9438.

LEGENDS

Table 1: Averages of S isotopic analyses of standards Canyon Diablo Troilite (CDT), IAEA-S1 and IAEA-S2. $\delta^{34}S$ is expressed vs. V-CDT, $\Delta^{33}S$ and $\Delta^{36}S$ are expressed vs. our SF6 tank. $\Delta'^{33}S$ and $\Delta'^{36}S$ are corrected values expressed vs. V-CDT. Standard deviations are given in 1σ.

Table 2: Sulfur and oxygen isotopic compositions of bulk fraction of enstatite chondrites and aubrites. δ34S is expressed vs. V-CDT, $\Delta'^{33}S$ and $\Delta'^{36}S$ are corrected values expressed vs. V-CDT. Individual analysis precision are standard deviation of 0.01 ‰ on $\delta^{33}S$ and $\delta^{34}S$ and 0.1 ‰ on $\delta^{36}S$ (1σ).

Table 3: Sulfur isotopic composition of the water soluble fraction of enstatite chondrites and aubrites. $\delta^{34}S$ is expressed vs. V-CDT, Δ'33S and Δ'36S are corrected values expressed vs. V-CDT. Individual analysis precision are standard deviation of 0.01 ‰ on δ33S and δ34S and 0.1 ‰ on δ36S (1σ).

Figure 1: Sulfur isotopic composition in the different groups of enstatite chondrites and aubrites. $\delta'^{34}S = 1000\ln(\delta^{34}S/1000+1)$, $\delta'^{33}S = 1000\ln(\delta^{33}S/1000+1)$. Δ'33S and Δ'36S are corrected values expressed vs. V-CDT

Figure 2: Δ'33S and Δ'36S compositions in the different groups of enstatite chondrites and aubrites. Δ'33S and Δ'36S are corrected values expressed vs. V-CDT.

Figure 3: Sulfur isotopic composition of the water soluble fraction in enstatite chondrites and aubrites. $\delta'^{34}S = 1000 \times \ln(\delta^{34}S/1000+1)$, $\delta'^{33}S = 1000 \times \ln(\delta^{33}S/1000+1)$

Figure 4: Δ'33S and Δ'36S compositions in the water soluble fraction of enstatite chondrites and aubrites. Spallation trend defined by Antonelli et al. (2014). Nebular trend defined by Farquhar et al. (2000). Photochemical trend defined by Chakraborty (2013). Δ'33S and Δ'36S are corrected values expressed vs. V-CDT.

Figure 5: Relation between δ34'S composition of the water soluble fraction and the concentration in CaS in enstatite meteorites. $\delta'^{34}S = 1000 \times \ln(\delta^{34}S/1000+1)$.

Appendix A: Replicate analyses of S isotopic analyses of standards Canyon Diablo Troilite (CDT), IAEA-S1 and IAEA-S2. $\delta^{34}S$ is expressed vs. V-CDT, $\Delta^{33}S$ and $\Delta^{36}S$ are expressed vs. our SF6 tank. $\Delta'^{33}S$ and $\Delta'^{36}S$ are corrected values expressed vs. V-CDT. Individual analysis precision are of 0.01 ‰ on $\delta^{33}S$ and $\delta^{34}S$ and 0.1 ‰ on $\delta^{36}S$ (1σ).

Table 1

Sample	**δ34S (‰)**	**Δ33S (‰)**	**Δ36S (‰)**	**Δ'33S (‰)**	**Δ'36S (‰)**
CDT (average)	**-0.377**	**-0.029**	**-0.129**	**0.000**	**0.000**
std. dev.	0.210	0.005	0.087	0.005	0.087
IAEA-1 (average)	**-0.296**	**0.088**	**-0.486**	**0.117**	**-0.357**
std. dev.	0.168	0.006	0.274	0.006	0.274
IAEA-2 (average)	**22.091**	**0.030**	**-0.197**	**0.059**	**-0.068**
std. dev.	0.395	0.075	0.298	0.075	0.298
IAEA-3 (average)	**-32.510**	**0.070**	**-0.501**	**0.099**	**-0.372**
std. dev.	0.063	0.007	0.260	0.007	0.260

Table 2

Sample	group	replica	**δ34S (‰)**	std dev. on replica (1σ)	**Δ'33S (‰)**	std dev. on replica (1σ)	**Δ'36S (‰)**	std dev. on replica (1σ)	**[S] (wt%)**	std dev. on replica (1σ)	**δ17O (‰)**	**δ18O (‰)**	**Δ17O (‰)**		**Exposure age based on H3 composition (Ma)**	
Sahara 97096	EH3	2	-0.136	*0.252*	-0.003	*0.001*	0.009	*0.042*	4.4	*0.51*	2.77	5.45	-0.07	(a)	9.00	(d)
Kota-Kota	EH3	2	-0.251	*0.166*	0.000	*0.002*	0.282	*0.146*	3.6	*0.09*	2.52	5.12	-0.15	(a)	36.50	(d)
Alha 77295	EH3	3	-0.312	*0.289*	-0.007	*0.005*	0.042	*0.062*	4.3	*0.13*	--	--	--			
Mil 07028	EH3	2	-0.400	*0.096*	0.007	*0.001*	-0.049	*0.046*	5.4	*0.31*	2.39	4.54	**-0.04**	(c)		
Gro 95517	EH3	5	-0.192	*0.169*	0.000	*0.004*	0.292	*0.062*	4.0	*0.18*	1.84	3.55	-0.02	(c)	35.10	(d)
Qingzhen	EH4	1	0.150	--	0.000	--	0.116	--	4.1	--	2.83	5.52	-0.04	(b)	1.90	(d)
Abee	EH4	6	-0.672	*0.289*	0.003	*0.009*	0.143	*0.059*	4.5	*0.86*	3.47	6.32	0.19	(a)	7.70	(d)
Indarch	EH4	3	-0.429	*0.140*	-0.002	*0.006*	-0.037	*0.046*	3.6	*0.81*	--	--	--		8.20	(d)
St. Mark's	EH5	5	-0.381	*0.120*	0.002	*0.005*	0.056	*0.108*	3.3	*0.90*	3.15	5.73	0.18	(a)	0.68	(d)
Saint-Sauveur	EH5	4	-0.025	*0.055*	0.004	*0.002*	0.027	*0.006*	5.2	*0.27*	--	--	--			
LAP 02 225	EH5	3	-0.062	*0.197*	0.004	*0.004*	0.008	*0.007*	2.4	*0.31*	--	--	--			
Itqiy	EH7-an	3	--	--	--	--	--	--	0.0	--	--	--	--			
MAC 88136	EL3	3	-0.469	*0.097*	0.007	*0.003*	0.009	*0.037*	2.2	*0.06*	2.01	4.07	-0.11	(b)	1.20	(d)
MAC 02837	EL3	3	-0.165	*0.090*	0.004	*0.004*	0.059	*0.015*	2.8	*0.23*	1.96	3.84	0.11	(c)		
Hvittis	EL6	2	-0.455	*0.089*	0.000	*0.016*	-0.160	*0.087*	2.4	*0.33*	3.02	5.68	0.07	(a)	18.90	(d)
Khairpur	EL6	1	-0.543	--	0.010	--	0.071	--	3.3	--	3.17	6.09	0.01	(b)		
Eagle	EL6	4	-0.642	*0.211*	0.008	*0.006*	-0.009	*0.071*	2.0	*0.60*	2.79	5.44	0.03	(c)	29.40	(d)
LON 94100	EL6	1	-0.721	--	-0.001	--	0.111	--	1.6	--	--	--	--		32.60	(d)
Pillistfer	EL6	1	-1.017	--	-0.007	--	-0.139	--	1.1	--	2.92	5.58	0.02	(a)	4.10	(d)
Atlanta	EL6	1	-0.521	--	0.008	--	0.024	--	2.3	--	2.96	5.63	0.03	(a)	32.30	(d)
Blithfield	EL6	1	-0.644	--	0.008	--	-0.035	--	4.9	--	2.82	5.29	0.07	(a)		
EET 92063	EL6	3	-0.655	*0.262*	-0.002	*0.005*	-0.024	*0.037*	1.8	*0.14*	3.06	5.84	0.03	(b)	35.30	(d)
NWA 974	EL6	3	-0.801	*0.173*	0.008	*0.003*	0.269	*0.041*	2.0	*0.57*	3.32	5.94	**0.22**	(c)		
North West Forest	EL6	1	--	--	--	--	--	--	0.0	--	--	--	--			
Happy Canyon	EL7	1	-0.637		-0.009		0.070		0.2	*0.07*					26.80	(d)
Ilafegh	EL7	3	-0.638	*0.564*	0.001	*0.006*	-0.085	*0.015*	0.5	*0.22*					3.80	(d)
Shallowater	Aubrites	1	-0.465		0.008		0.319		2.8	--	2.99	5.79	-0.02	(b)	0.28	(f)
Bishopville	Aubrites	1	-1.350	*0.783*	0.021	*0.010*	0.094	*0.011*	1.0	*0.88*	2.59	5.09	0.09	(b)	52.5	(f)
Bishopville	Aubrites	1	0.215	--	0.000	--	0.117	--	--	--	--	--	--			
Norton County	Aubrites	1	-1.150	--	-0.008	--	0.023	--	0.6	*0.13*	2.57	4.98	-0.02	(b)	117.4	(f)
Aubres	Aubrites	1	0.451	--	-0.003	--	-0.027	--	0.3	--	--	--	--			
Bustee	Aubrites	4	-0.189	*0.080*	0.008	*0.001*	-0.006	*0.040*	0.1	*0.01*	--	--	--		50.8	(f)
Khor Temiki	Aubrites	1	-0.154	--	0.013	--	0.020	--	0.3	--	--	--	--		53.9	(f)
Mayo Belwa	Aubrites	1	-0.404	--	0.007	--	-0.083	--	0.2	--	--	--	--		102.4	(f)
Pena Blanca Spring	Aubrites	1	-0.766	--	0.008	--	-0.033	--	--	--	--	--	--		69.5	(f)
Cumberland Falls	Aubrites	2	-0.517	*0.068*	0.011	*0.003*	-0.015	*0.014*	1.5	*0.95*	3.36	5.44	0.53	(b)		
Cumber. (Aubrite clast)	Aubrites	1	-1.903	--	0.017	--	0.078	--	0.1	--	--	--	--			
Cumber. (chondrite clast)	Aubrites	1	0.007	--	0.006	--	0.089	--	0.9	--	--	--	--			

(a) Clayton et al. 1884 (b) Newton et al. 2000 (c) this study (d) Patzer & Schultz 2001 (f) Lorenzetti 2003

Table 3

Sample	group	replica	**δ34S (‰)**	**Δ'33S (‰)**	**Δ'36S (‰)**	**%CaS in S (wt%)**
Abee	EH3/4	1	2.477	-0.015	0.061	3.1
Indarch	EH3/4	1	4.503	0.006	2.229	0.1
St Mark's	EH5	1	0.666	-0.004	0.058	9.3
St Sauveur	EH5	1	0.903	-0.003	0.178	4.8
Aubres	Aubrites	1	2.219	-0.025	0.906	0.7
Bustee	Aubrites	1	4.149	-0.037	0.065	61.9
Mayo Belwa	Aubrites	1	5.370	-0.028	0.348	3.5
Norton County	Aubrites	1	10.946	-0.085	1.185	1.2
Pena Blanca Spring	Aubrites	1	1.324	0.011	-0.048	--
Cumberland Falls	Aubrites	1	--	--	--	0.0
Bishopville	Aubrites	1	--	--	--	0.0
Khor Temiki	Aubrites	1	--	--	--	0.0

Figure 1

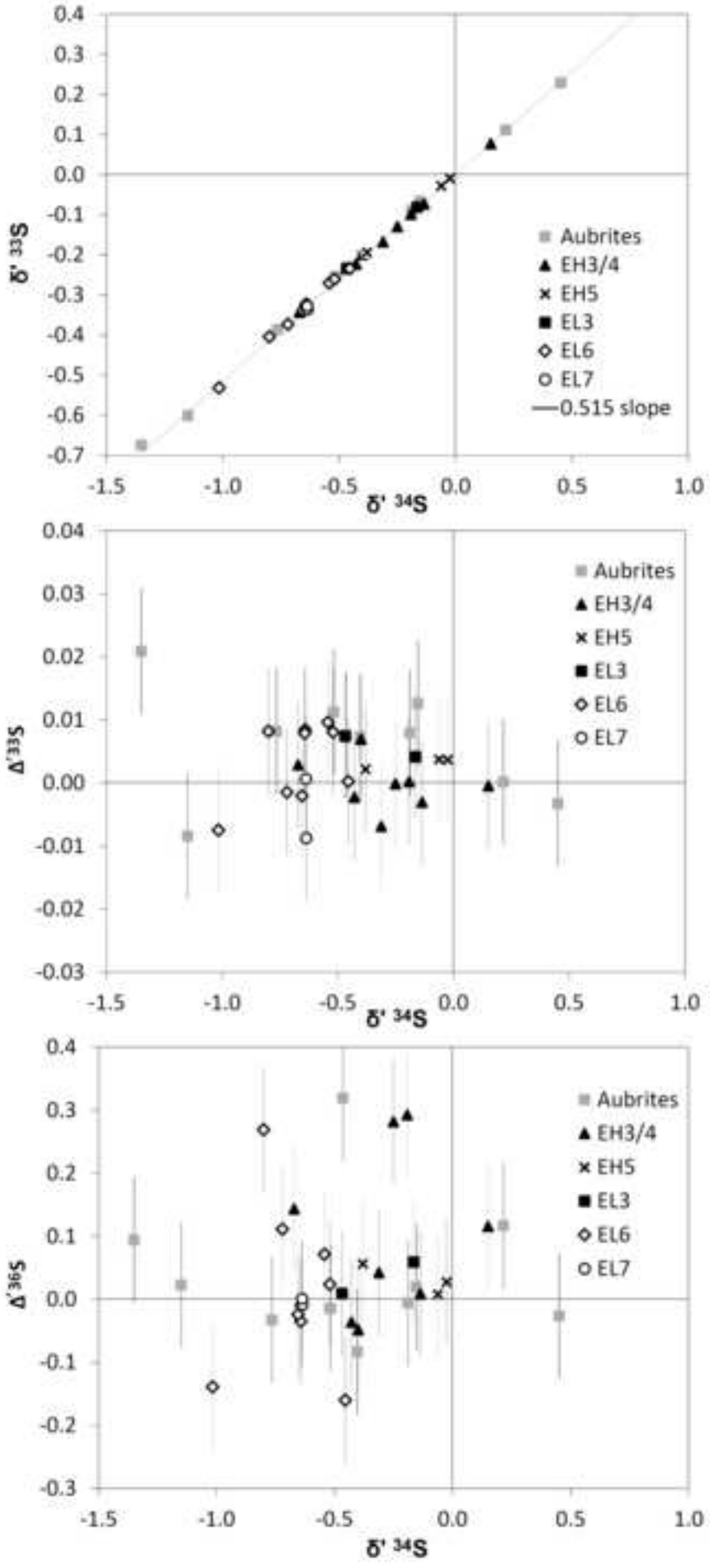


Figure 2

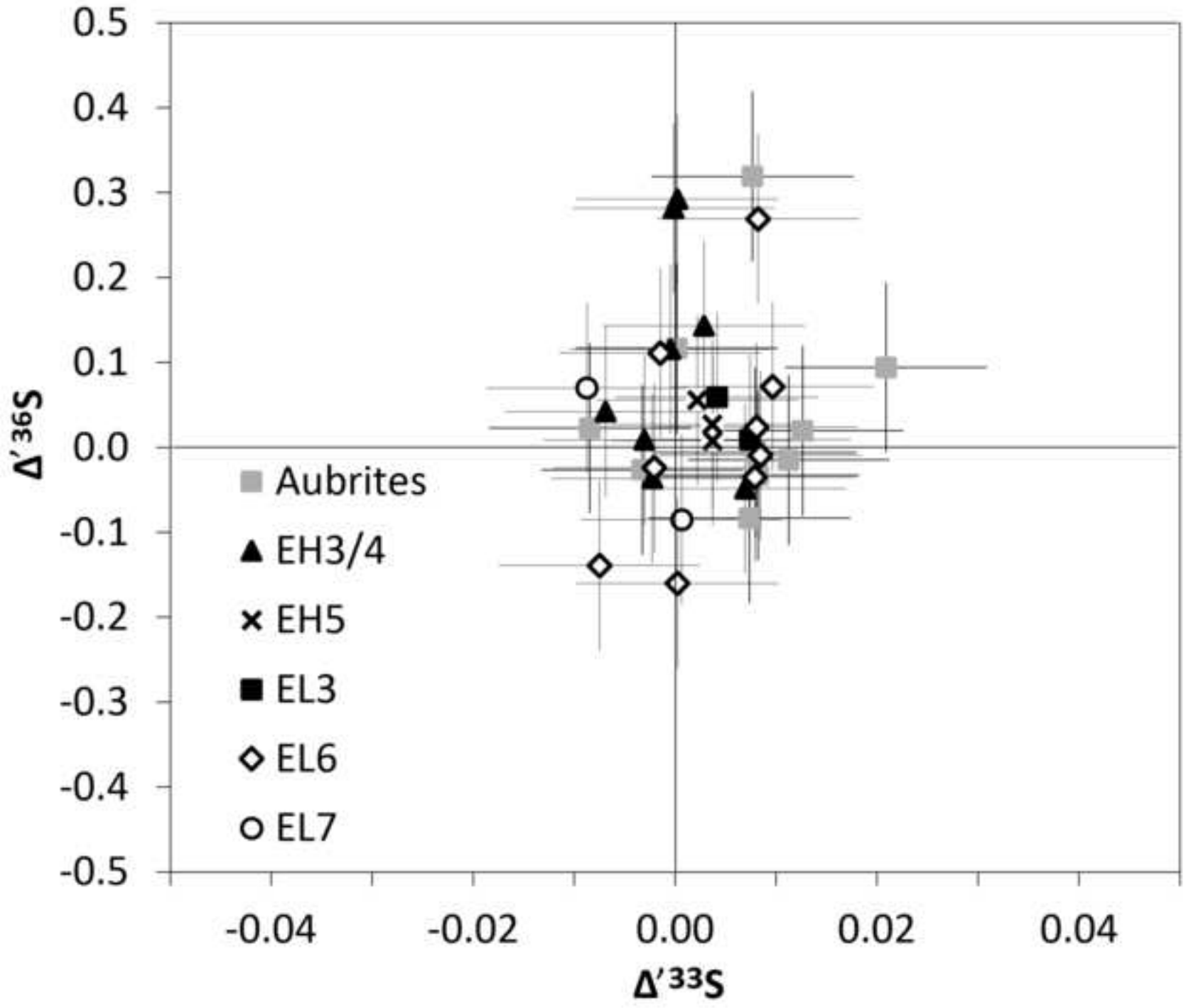

0.5
0.4
0.3
0.2
0.1
0.0
-0.1
-0.2
-0.3
-0.4
-0.5
Δ'36S
Aubrites
EH3/4
EH5
EL3
EL6
EL7
-0.04
-0.02
0.00
0.02
0.04
Δ'33S

Figure 4

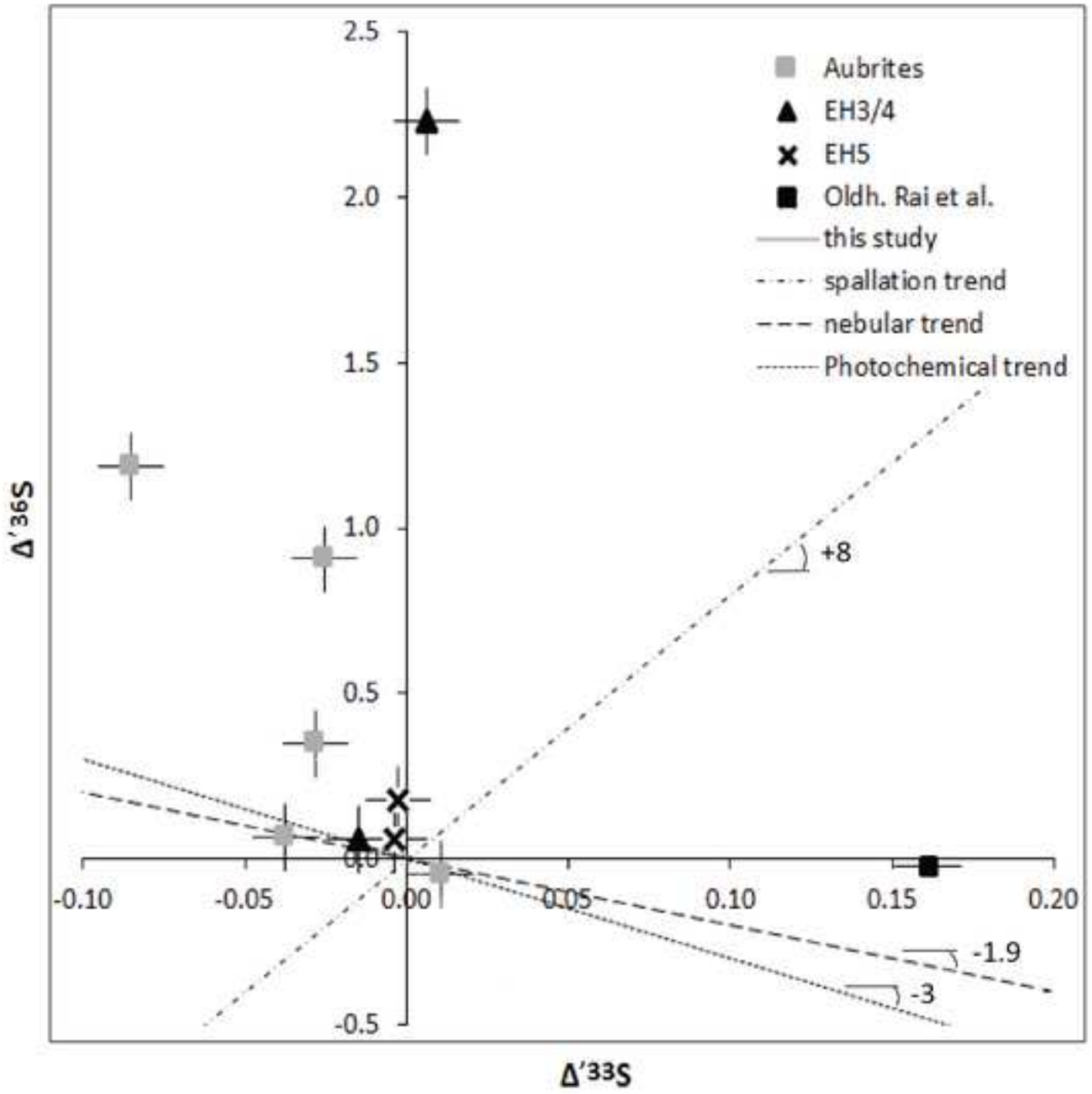
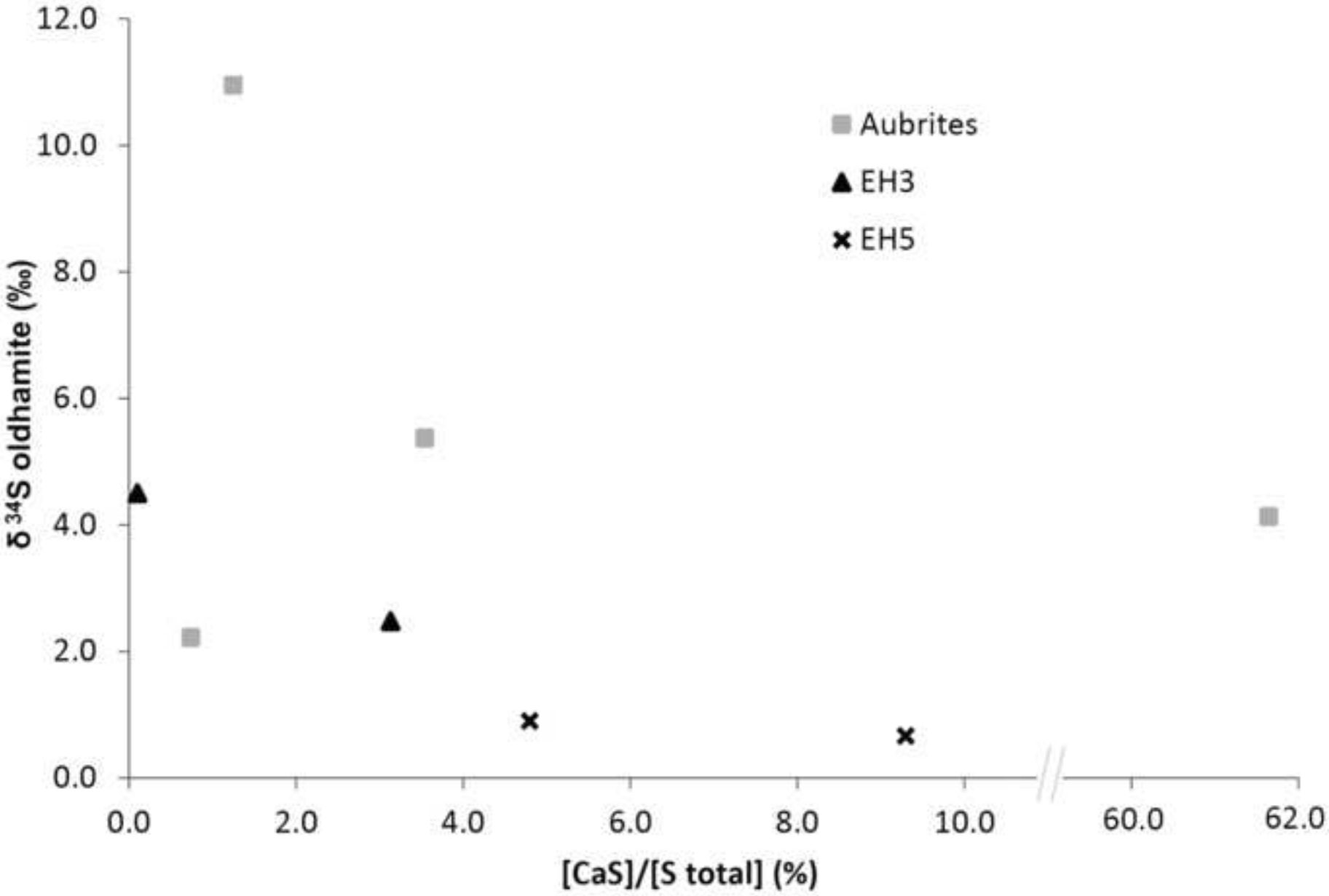

Aubrites
EH3/4
EH5
Oldh. Rai et al.
this study
spallation trend
nebular trend
Photochemical trend
+8
-1.9
-3
2.5
2.0
1.5
1.0
0.5
0.0
-0.5
-0.10
-0.05
0.00
0.05
0.10
0.15
0.20
Δ'36S
Δ'33S

Figure 5


12.0
10.0
8.0
6.0
4.0
2.0
0.0
δ 34S oldhamite (‰)
Aubrites
EH3
EH5
0.0
2.0
4.0
6.0
8.0
10.0
60.0
62.0
[CaS]/[S total] (%)